JOURNAL OF GEOPHYSICAL RESEARCH, VOL. 112, B07318, doi:10.1029/2006JB004861, 2007

Lithospheric variations across the Superior Province, Ontario, Canada: Evidence from tomography and shear wave splitting

A. W. Frederiksen,[1] S.-K. Miong,[2] F. A. Darbyshire,[3] D. W. Eaton,[4] S. Rondenay,[5] and S. Sol[6]

Received 16 November 2006; revised 23 April 2007; accepted 17 May 2007; published 31 July 2007.

[1] The Superior Province of the Canadian Shield is the largest contiguous region of the Archean crust. A combination of data from multiple experiments is used to obtain shear wave splitting parameters and a three-dimensional tomographic velocity model beneath a large portion of the Superior, corresponding approximately to the province of Ontario. Shear wave splits are obtained at 24 sites across the Superior, displaying strong (averaging 1.34 s) ENE-WSW splitting at stations west of 86°W and weaker (0.67 s) E-W splitting in the east. The fast direction is subparallel to both absolute plate motion and tectonic belt boundaries. The recovered tomographic velocity model shows a major boundary oriented NNW-SSE, separating high velocities in the western Superior (WS) from low velocities in the east and coinciding with the divide between weak and strong shear wave splits. Other features include a 200-km-thick low-velocity anomaly corresponding to the Nipigon Embayment, a 1.0-Ga failed-rift branch; and a linear low-velocity anomaly in the east, attributed to the Great Meteor hot spot track. The Nipigon anomaly, in the western portion of the model, is probably in situ, while the Great Meteor track is displaced from crustal features associated with the hot spot. We interpret this displacement as evidence that the eastern lithosphere has been deformed by basal drag, while the western lithosphere has remained stable, and propose that the east-west lithospheric boundary we have detected represents a change in mechanical properties, between stronger, higher velocity western material with consistent anisotropic fabric, and weaker eastern material with more variable fabric.

Citation: Frederiksen, A. W., S.-K. Miong, F. A. Darbyshire, D. W. Eaton, S. Rondenay, and S. Sol (2007), Lithospheric variations across the Superior Province, Ontario, Canada: Evidence from tomography and shear wave splitting, *J. Geophys. Res.*, *112*, B07318, doi:10.1029/2006JB004861.

1. Introduction

[2] The remarkable stability of Archean cratons has been attributed to the presence of an underlying thick-mantle lithosphere [e.g., *Jordan*, 1978], particularly given the ubiquity of high-velocity tomographic anomalies beneath shield regions. Several models for the origin of this lithosphere have been proposed [see e.g., *Jordan*, 1988, *Pearson*, 1999], including advective thickening, underplating, progressive accretion (either laterally or via shingled subduction), and rapid formation via subduction or plume activity. These models have different implications for the age of the continental lithosphere and its relationship to overlying crustal domains. Though seismic imaging is not a direct measure of age or lithology, it is a suitable method for detecting large-scale lithospheric mantle structures and determining the degree to which they correlate with crustal terranes.

[3] The high seismic velocity of stable continental lithosphere is commonly attributed to the presence of low-temperature, depleted mantle. Though stable continental regions are generally underlain by high-velocity mantle, localized low-velocity features have been found within the continental lithosphere. Such features would require a thermal or chemical contrast with surrounding material [*Sobolev et al.*, 1996], through the incorporation of more enriched or higher temperature mantle, or localized thinning of the continental lithosphere. Low-velocity features beneath cratons have in several cases been attributed to hot spot activity heating, eroding, or modifying the litho-

[1]Department of Geological Sciences, University of Manitoba, Winnipeg, Manitoba, Canada.
[2]Department of Geology and Geophysics, University of Calgary, Calgary, Alberta, Canada.
[3]Département des sciences de la terre et de l'atmosphere, Université du Québec à Montréal, Montréal, Québec, Canada.
[4]Department of Earth Sciences, University of Western Ontario, London, Ontario, Canada.
[5]Department of Earth, Atmospheric, and Planetary Sciences, Massachusetts Institute of Technology, Cambridge, Massachusetts, USA.
[6]Department of Earth and Environmental Sciences, Lehigh University, Bethlehem, Pennsylvania, USA.

0148-0227/07/2006JB004861$09.00

sphere [see e.g., *VanDecar et al.*, 1995; *Rondenay et al.*, 2000a, 2000b].

[4] In regions without thick lithosphere, shear wave splitting is most commonly attributed to lattice-preferred orientation induced by strain within the actively deforming asthenosphere, the crustal contribution being comparatively small. The thick, stable lithosphere beneath cratons is capable of preserving a significant thickness of frozen fabric [*Silver and Kaneshima*, 1993], representing fossil rather than active strain. Such fossil strain would presumably record the tectonic history of the lithosphere and would reflect crustal tectonics inasmuch as the crust and mantle are coupled. If the asthenospheric and lithospheric fabrics are not parallel, the recorded shear wave splitting will record the interfering effects of both [*Levin et al.*, 1999].

[5] The Superior Province, the largest Archean province in the world, has been stable for ≈2.6 Ga and is underlain by high-velocity upper mantle imaged by several continental surface-wave models [e.g., *Godey et al.*, 2003; *Van der Lee and Frederiksen*, 2005]. The internal structure of the Superior lithosphere is coarsely resolved in these models, though there are suggestions of lateral variations across the province. More localized mantle studies [*Rondenay et al.*, 2000a, 2000b; *Sol et al.*, 2002] revealed the presence of small-scale high- and low-velocity structures within regions of the Superior Province (including a possible hot spot feature) but did not address east-west velocity variations across the craton. Differences in shear wave split times between the Abitibi region [*Rondenay et al.*, 2000a, 2000b; *Frederiksen et al.*, 2006] and the western Superior [*Kay et al.*, 1999] suggest substantial differences in upper mantle structure, but the large gap in coverage in central Ontario leaves the transition unresolved. With the advent of Federal Economic Development Initiative for Northern Ontario (FedNor) instrumentation [*Darbyshire et al.*, 2006] providing broad coverage across Ontario, it is now possible to fill this gap and obtain three-dimensional structure and SKS splitting measurements over a large fraction of the Superior Province.

2. Structure and History of the Superior Province

[6] The Superior Province is exposed beneath northwestern Quebec, central and western Ontario, western Manitoba, and northern Minnesota (Figures 1a and 1b) and is interpreted to extend beneath sedimentary cover to the north, west, and south [*Card and Poulsen*, 1998]. The exposed portion of the Superior Province has been divided into subprovinces believed to represent distinct terranes or terrane complexes; their boundaries generally trend east-west and are more closely spaced in the western Superior (Figure 1b). The northern Superior contains a high proportion of ca. 3.0-Ga rocks, and the subprovinces are generally believed to display younger ages southwards, resulting from a 500-Ma period of accretion in the Mesoarchean and Neoarchean in a Pacific-like setting [*Williams et al.*, 1991; *Card and Poulsen*, 1998]. Final docking of the terranes forming the Superior is believed to have taken place from north to south in the Kenoran Orogeny at 2.72–2.69 Ga. This assembly was accompanied and followed by extensive plutonism and crustal thickening [*Williams et al.*, 1991; *Card and Poulsen*, 1998], generating a thick, depleted mantle root.

[7] The Superior Province has been virtually quiescent since the end of the Archean. A notable exception is the Kapuskasing Structural Zone (KSZ), a narrow high-grade region of intracratonic uplift, thrusting, and crustal thickening running from eastern Lake Superior to James Bay (Figure 1b), in which a cross-section of Archean crust is exposed. Activity on the KSZ occurred in multiple stages beginning ca. 2.5 Ga [*Percival and West*, 1994; *Card and Poulsen*, 1998]. A major episode of compressional KSZ deformation is interpreted in the early Proterozoic (1.95–1.85 Ga), while late faulting is believed to have taken place at ca. 1.1 Ma [*Percival and West*, 1994]. The Superior also hosts more than twelve Proterozoic dyke swarms, including the 2.45-Ga Matachewan and Hearst swarms over much of Ontario, the 1.88-Ga Molson swarm in the northwest Superior, and the 1.2- to 1.1-Ga Keweenawan swarm surrounding the western Lake Superior [*Green et al.*, 1987; *Osmani*, 1991; *Card and Poulsen*, 1998].

[8] The Superior Province is bounded by Proterozoic orogens on all sides. Excluding northeastern Quebec, which is outside of our study area, the provinces bounding the Superior are, from oldest to youngest, the Trans-Hudson, Southern, and Grenville provinces (Figure 1a). The margin with the Trans-Hudson orogen, at the northwest edge of the Superior, is believed to have been a passive margin at ca. 2.1–2.0 Ga, becoming convergent from 1.92 to 1.83 Ga and collisional from 1.83 to 1.68 Ga [*Lucas et al.*, 1998]. The Southern Province, south and southeast of the Superior, includes passive margin rocks with ages from 2.4 to 1.7 Ga, affected by the 1.8-Ga Penokean Orogeny [*Thurston*, 1991]. The Grenville Province, southeast of the Superior, represents a multistage orogeny occurring from 1.3 to 1.0 Ga, which was the last major accretionary event forming the Canadian Shield [*Davidson*, 1998].

[9] Overlapping with Grenvillian orogenesis, the Midcontinent Rift, a very large continental rift structure, developed across the Southern Province at 1.11–1.09 Ga, forming an arcuate belt more than 2000 km long [*Sutcliffe*, 1991; *Davidson*, 1998]. The rift developed as a series of half-grabens which thinned the crust extensively and are filled with up to 30 km of sedimentary and volcanic rocks [*Sutcliffe*, 1991]. In the Lake Superior area, these deposits form the Keweenawan Supergroup, which includes large quantities of basalt. The Nipigon Embayment, north of Lake Superior, contains diabase sills found to be approximately contemporaneous with Lake Superior Keweenawan tholeiites; given its location at a major bend in the Midcontinent Rift, the embayment is believed to represent a failed branch of the rift [*Sutcliffe*, 1991].

3. Previous Geophysical Studies

[10] A number of geophysical studies have been undertaken to relate lithospheric structure to crustal architecture and history of the Superior Province, largely under the auspices of LITHOPROBE [*Clowes et al.*, 1992]. From west to east, the transects intersecting the Superior were the western Superior (WS), Kapuskasing Structural Zone (KSZ), and Abitibi-Grenville (AG); the Great Lakes (GL) transect took place in the adjacent Southern Province.

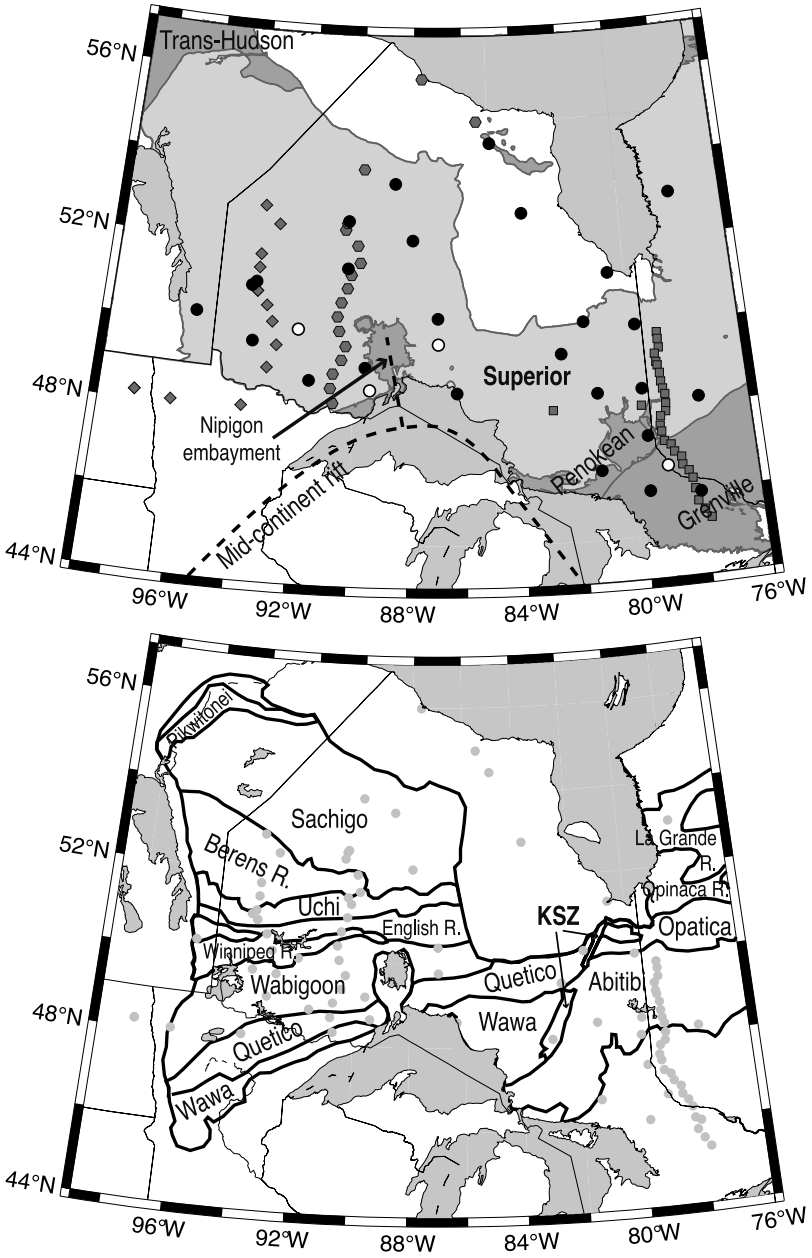

Figure 1. (a) Map of stations used in this study, overlain on tectonic province boundaries (boundaries from Geological Survey of Canada Web site, covering Canada only; white regions within Canada indicate Phanerozoic cover). Gray symbols indicate previous temporary deployments: APT89 (diamonds), TW∼ST (hexagons), and Abitibi 1996 (squares); circles are stations of the FedNor, CNSN, and POLARIS networks (hollow: short-period; filled: broadband). For details of the latter stations, see Table 1. (b) Subprovinces of the Superior, digitized from *Card and Poulsen* [1998]. KSZ: Kapuskasing Structural Zone.

Seismic reflection [*White et al.*, 2003; *Calvert et al.*, 2004] and refraction [*Musacchio et al.*, 2004] studies of the WS transect were used to infer crustal-scale sutures reaching the Moho, supporting an accretionary model for the formation of the Superior Province. Subcrustal reflectivity and subcrustal layering were suggested to represent relict oceanic lithosphere. Similar sutures and subcrustal features were also inferred via reflection along the AG transect [*Calvert et al.*, 1995; *Calvert and Ludden*, 1999], though they have also been interpreted to represent lower crustal delamination [*Benn*, 2006]. By contrast, the Kapuskasing Structural Zone does not exhibit Moho-crossing reflections [*Wu and Mereu*, 1992].

[11] LITHOPROBE studies of the Superior Province were not limited to controlled-source seismology. Passive seismic array studies in the region of the WS transect [*Kay et al.*, 1999; *Sol et al.*, 2002] detected strong E-W fabric (consistent with an earlier study by *Silver and Kaneshima* [1993]) as well as a northeast-dipping, tabular high-velocity anomaly west of Lake Nipigon, interpreted to be remnant-

subducted lithosphere. An experiment along the AG transect [*Rondenay et al.*, 2000a, 2000b] detected a low-velocity channel attributed to the track of the Great Meteor hot spot across the continental lithosphere; SKS splits were found to be variable and weaker than in the WS [*Frederiksen et al.*, 2006]. Magnetotelluric soundings in the western Superior [*Ferguson et al.*, 2005] detected dominant east-west geoelectric strikes at frequencies corresponding to lithospheric depths, as well as an anomalous phase response beneath the Nipigon Embayment; surveys on the AG transect [*Boerner et al.*, 2000; *Frederiksen et al.*, 2006] found changes in electrical anisotropy across the Abitibi and Kapuskasing regions.

4. Data Set

[12] The first teleseismic array deployed on the Superior Province was the 1989 Archean-Proterozoic Transition (APT89) seismic experiment [*Silver et al.*, 1993], which included an approximately north-south line near the western border of Ontario (Figure 1a, diamonds); these data were analyzed for SKS splitting [*Silver and Kaneshima*, 1993] and traveltime residuals [*Bokelmann and Silver*, 2000], but traveltime tomography was not performed. The LITHOPROBE Abitibi-Grenville and western Superior transects each inspired teleseismic experiments, the 1994 and 1996 Abitibi experiments [*Rondenay et al.*, 2000b] (Figure 1a, squares) and the 1997 Teleseismic Western Superior Transect (TW∼ST) experiment [*Kay et al.*, 1999] (Figure 1a, hexagons). Data from each of these experiments have been analyzed for shear wave splitting [*Ji et al.*, 1996; *Kay et al.*, 1999; *Rondenay et al.*, 2000a, 2000b] as well as traveltime tomography [*Rondenay et al.*, 2000a, 2000b; *Sol et al.*, 2002]. As a result of these studies, the mantle beneath the southeastern and western edges of the Superior has been characterized with a high level of detail; however, because of the absence of constraints from central Ontario, it is difficult to assemble a large-scale picture of the mantle beneath the Superior Province.

[13] The Portable Observatories for Lithospheric Analysis and Research Investigating Seismicity (POLARIS) project [*Eaton et al.*, 2005] includes two broadband deployments in Ontario: the dense POLARIS Ontario deployment in southern Ontario and the broader scale FedNor deployment across the rest of the province. The POLARIS Ontario array is restricted to the Proterozoic Grenville Province and has already been analyzed using shear wave splitting [*Eaton et al.*, 2004] and tomographic [*Aktas and Eaton*, 2006] techniques; apart from a few northern stations, it is omitted from this study. The FedNor array, however, lies entirely within the Superior Province [*Darbyshire et al.*, 2006], including regions not sampled by previous studies (Figure 1a, circles); in combination with adjacent permanent Canadian National Seismograph Network (CNSN) short-period and broadband stations, the FedNor array opens up the possibility of examining a large portion of the Superior craton at once. Data from the FedNor array have been the subject of surface-wave studies for lithospheric structure [*Darbyshire et al.*, 2006], but no traveltime or shear wave splitting studies have been published. In this study, we present shear wave splitting analyses for stations of the FedNor array and combine new traveltime picks from FedNor, CNSN, and APT89 data (the latter obtained from the Incorporated Research Institutions for Seismology (IRIS) data management center) with the existing set of traveltime picks from the TW∼ST and Abitibi arrays [*Rondenay et al.*, 2000a, 2000b; *Sol et al.*, 2002], obtaining a three-dimensional velocity model of the mantle beneath a major part of the Superior Province. Further information on the instruments used in this study is given in Table 1; for more detail, see *Darbyshire et al.* [2006].

5. Shear Wave Splitting

5.1. Method

[14] Splitting of core-refracted *S* waves provides unambiguous evidence of receiver-side anisotropy and is generally assumed to result largely from upper mantle fabric [*Silver and Chan*, 1991]. The commonly given splitting parameters are the delay time between fast and slow quasi-shear waves, and the polarization direction of the fast wave, though these parameters implicitly assume a single anisotropic layer with a horizontal axis of symmetry. A number of methods for measuring split times and fast directions exist, but tend to give similar results in practice. We studied SKS, SKKS, and SKiKS phases in the 0.02- to 0.2-Hz frequency band and found the splitting parameters by minimizing the second eigenvalue of the covariance matrix between the corrected traces [*Silver and Chan*, 1991], a technique which is robust given variations in the polarization of the incident wave. As a cross-check, we also minimized the transverse-component energy, which gave comparable results.

[15] Standard approaches to shear wave splitting analysis assume that the receiver-side structure may be approximated to be a single layer of anisotropic material. Multiple layers of anisotropy with differing fast-axis orientations lead to systematic variations in splitting parameters with back azimuth [*Levin et al.*, 1999]. Plotting split parameters against back azimuth generally did not reveal such variation, though the scatter in the recovered parameters was considerable. To explore this issue in more detail, we stacked error surfaces (in the manner of *Wolfe and Silver* [1998]) for events in 10° back-azimuthal swathes (see Figure 2 for an example). Though the shapes of the error surfaces vary considerably with back azimuth, the single-layer parameters obtained from the whole data set generally plot in low-error regions in all back-azimuthal swathes, indicating that one-layer models are consistent with the data set for all stations. We cannot rule out the presence of multiple anisotropic layers, but a single-layer approach is sufficient to explain our observations.

[16] Having established that single-layer models are acceptable for these stations, we found one-layer splitting parameters by stacking error surfaces for all back azimuths. In order to compensate for the uneven back-azimuthal distribution of the available events, we stacked the error surfaces in two stages, first stacking single-event surfaces in the aforementioned back-azimuthal swathes 10° wide then stacking the composite error surfaces for each swath with equal weighting. This procedure is expected to give a result close to the true mean value in the presence of back-azimuthal variation. The results (Table 1) show significant anisotropy at every station examined; splitting parameters

Table 1. CNSN, POLARIS, and FedNor Stations Used in This Paper[a]

Station	Affiliation	Latitude, °	Longitude, °	Fast axis, °	Split time, s	Number of events
ALGO[b]	POLARIS	45.954	−78.051	109 ± 32	0.40 ± 0.30	9 SKS
ATKO	FedNor	48.823	−91.600	67 ± 8	1.23 ± 0.38	8 SKS, 4 SKKS
EEO	CNSN	46.641	−79.073	–	–	–
EPLO	FedNor	49.674	−93.736	64 ± 6	1.78 ± 0.33	7 SKS, 4 SKKS
GTO	CNSN	49.756	−86.961	–	–	–
HSMO[c]	FedNor	47.371	−79.666	84 ± 18	0.58 ± 0.40	5 SKS, 2 SKKS, 1 SKiKS
KAPO[d]	CNSN	49.450	−82.508	69 ± 11	0.58 ± 0.23	7 SKS, 9 SKKS
KASO	FedNor	53.528	−88.641	89 ± 21	0.93 ± 0.53	9 SKS, 4 SKKS
KILO[d]	FedNor	48.497	−79.723	70 ± 13	1.10 ± 0.63	12 SKS, 15 SKKS
LDIO	FedNor	49.175	−89.596	76 ± 19	0.70 ± 0.33	9 SKS, 3 SKKS
MALO[d]	FedNor	50.024	−79.764	89 ± 13	0.98 ± 0.38	8 SKS, 9 SKKS
MSNO	FedNor	51.291	−80.611	68 ± 14	0.83 ± 0.65	2 SKS, 1 SKKS
MUMO	FedNor	52.613	−90.391	82 ± 11	1.10 ± 0.35	10 SKS, 5 SKKS
NANO	FedNor	50.354	−86.968	71 ± 16	0.83 ± 0.58	10 SKS, 5 SKKS, 1 SKiKS
NSKO	FedNor	52.197	−87.931	86 ± 19	0.83 ± 0.58	5 SKS, 4 SKKS, 1 SKiKS
OTRO[d]	FedNor	50.182	−81.629	63 ± 14	0.75 ± 0.35	5 SKS, 10 SKKS
PKLO	FedNor	51.499	−90.352	75 ± 8	1.20 ± 0.33	11 SKS, 9 SKKS
PNPO	FedNor	48.596	−86.285	97 ± 18	0.70 ± 0.25	8 SKS, 5 SKKS
RDLO	FedNor	50.974	−93.912	66 ± 8	1.45 ± 0.35	4 SKS, 3 SKKS
RLKO	FedNor	51.070	−93.758	75 ± 13	1.40 ± 0.68	9 SKS, 7 SKKS, 1 SKiKS
RSPO	POLARIS	46.073	−79.760	–	–	–
SILO	FedNor	54.479	−84.913	81 ± 18	0.35 ± 0.30	7 SKS, 4 SKKS
SOLO	CNSN	50.021	−92.081	–	–	–
SUNO[d]	FedNor	46.644	−81.344	86 ± 12	0.88 ± 0.33	10 SKS, 14 SKKS
TBO	CNSN	48.647	−89.408	–	–	–
TIMO	FedNor	48.466	−81.303	74 ± 11	0.78 ± 0.40	5 SKS, 2 SKKS, 1 SKiKS
ULM	CNSN	50.250	−95.875	59 ± 7	1.73 ± 0.38	17 SKS, 10 SKKS
VIMO	GSC-NRD	52.817	−83.745	74 ± 12	0.93 ± 0.38	13 SKS, 10 SKKS
VLDQc	CNSN	48.190	−77.757	89 ± 8	0.83 ± 0.28	7 SKS, 10 SKKS
WEMQ	GSC-NRD	53.054	−77.974	65 ± 52	0.75 ± 0.65	4 SKS, 5 SKKS

[a]Stations with no split parameters are short-period vertical instruments (except for RSPO). Station affiliations are the following: CNSN: permanent Canadian National Seismograph Network observatories; POLARIS: Portable Observatories for Lithospheric Analysis and Research Investigating Seismicity, FedNor: extension of the POLARIS network funded by the Federal Economic Development Initiative for Northern Ontario, GSC-NRD: Geological Survey of Canada Northern Resources Development. The FedNor stations are jointly affiliated with the GSC-NRD.

[b]Split time determined by *Eaton et al.* [2004].

[c]Horizontal components incorrectly oriented; rotation correction of −36° applied.

[d]Split times previously presented by *Frederiksen et al.* [2006].

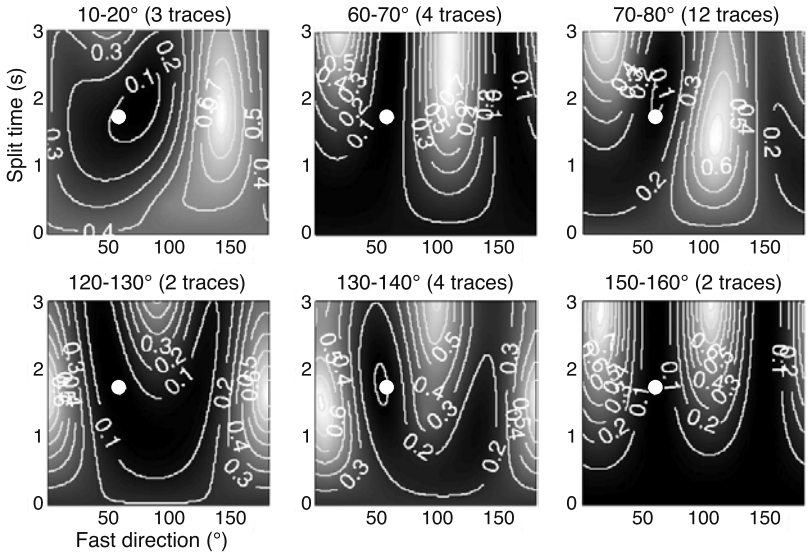

Figure 2. Stacked, normalized error surfaces for SKS splitting parameters at station ULM, plotted by back-azimuthal swath (with unpopulated swaths excluded). Each swath includes events lying in a 10° band of back azimuths, as well as events from a band 180° away which will exhibit the same incident polarization. The final single-layer model (white circle) lies in low-error (black) regions for all sampled swaths, indicating that a single-layer solution is consistent with the data set. Similar results were found for other stations.

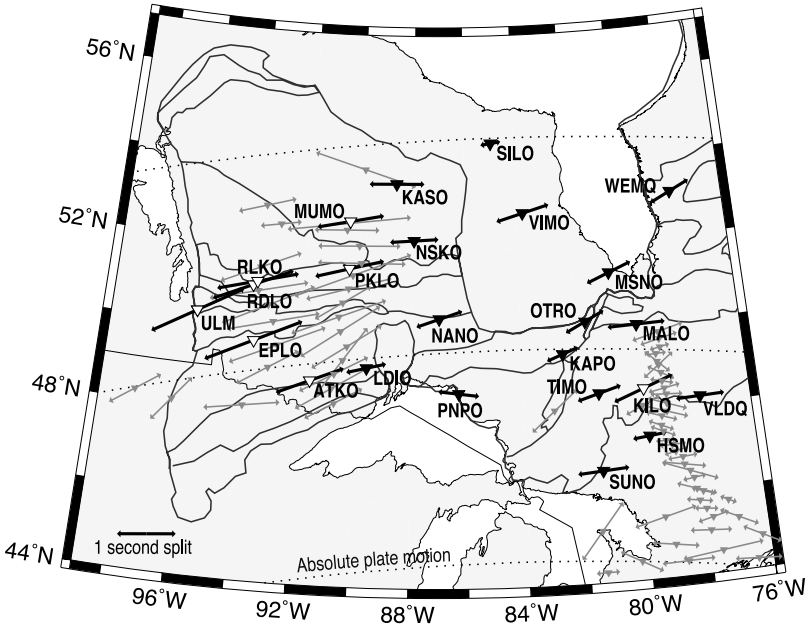

Figure 3. SKS splitting results over the study area. Results from previous experiments [*Silver and Kaneshima*, 1993; *Kay et al.*, 1999; *Rondenay et al.*, 2000a, 2000b; *Eaton et al.*, 2004] are shown as gray arrows; black arrows are results for POLARIS, FedNor, and CNSN stations in this study. White triangles indicate stations with split times of 1 s or more. Solid black lines are subprovince boundaries from Figure 1b; dotted lines indicate the direction of absolute plate motion, drawn as small circles around the Euler pole [*Larson et al.*, 1997].

for six of these stations were previously presented by *Frederiksen et al.* [2006].

5.2. Results

[17] Final composite SKS splitting parameters are given in Table 1 and plotted in Figure 3 along with the previously published results mentioned above. The most obvious spatial variation is between the western and eastern portions of the study area. The largest split detected, station EPLO at 1.78 s, is within the western Superior; the weakest split, at station SILO, is 0.35 s, which is barely significant given the 95% confidence limit of ±0.30 s. SILO is located on the Sutton Inlier, a small region of exposed Trans-Hudson bedrock, and thus lies outside of the Superior Province.

[18] As shown in Figure 4, there is a large decrease in split times east of ≈86°W, the average split time dropping by half from 1.34 to 0.67 s. The location and sharpness of the boundary are not well-constrained, given that there are relatively few stations between 84° and 88°W. There is also a change in fast-axis orientation from west to east, the mean fast direction changing from ENE (70.7°) west of 86°W to E (89.8°) east of 86°W; though the fast directions in the west are fairly tightly clustered, those in the east show considerable scatter (as evidenced by an increase in standard deviation from 14.7 to 19.9°).

6. Teleseismic Tomography

6.1. Method

[19] Teleseismic traveltime tomography is a well-established approach to obtaining three-dimensional mantle structure. It is based on the principle that waves traveling from distant earthquakes to localized station arrays travel along an approximately common path near the source, diverging in the mantle beneath the receivers. As a result, variations in arrival time between stations may be assumed to reflect receiver-side rather than source-side structure. Earthquakes in the teleseismic range (≈30–100° from the receiver) are ideal for the purpose because of their simple raypaths, avoiding both triplications and core interactions.

[20] We use a teleseismic tomography technique developed by *VanDecar* [1991]. The method solves for a three-dimensional *P* velocity model parameterized as a deviation from the IASP91 standard Earth model [*Kennett and Engdahl*, 1991], specified on grid nodes interpolated by splines under tension. The grid nodes are specified in spherical coordinates, in this case, from 42°N to 58°N, 74°W to 100°W, and to a maximum depth of 1000 km. A grid spacing of 0.333° in latitude, 0.5° in longitude, and 33.3 km in depth was used (except at the edges of the model where resolution is poor) for a total of 41 × 49 × 28 grid nodes. The inversion thus involves solving for 56,252 unknowns (along with station and event corrections), using smoothing and flattening regularization to compensate for the underdetermined nature of the problem. The correct level of regularization was determined somewhat subjectively by examining the trade-off between model roughness and data misfit; in the absence of good constraints on the noise level, the point of greatest curvature on a trade-off curve between roughness and misfit may be used to approximate the noise level [*Parker*, 1994].

6.2. Traveltime Measurements

[21] The four data sets (FedNor/CNSN, APT89, Abitibi, and TW∼ST) do not overlap in time. Therefore their event

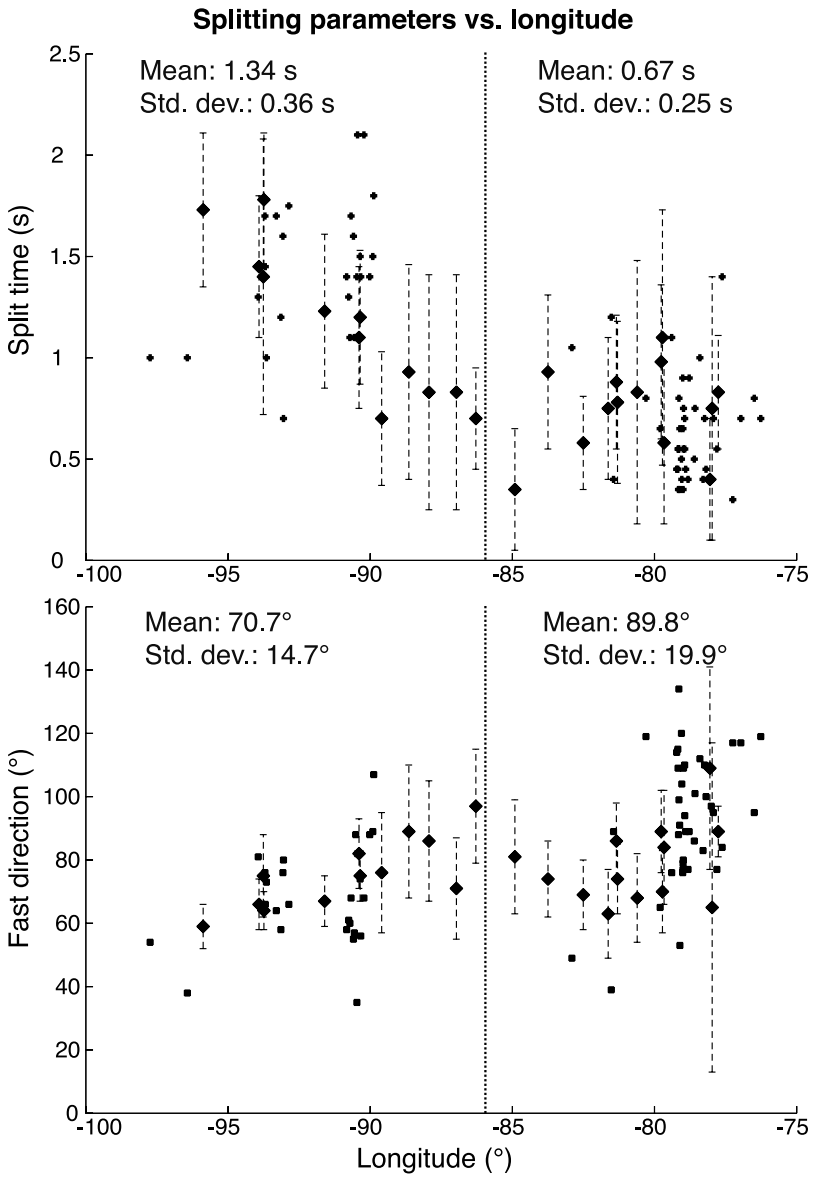

Figure 4. Splitting parameters for the study area, plotted against longitude. All results shown in Figure 3 are included; those with error bars are from this study. The means and standard deviations shown are for stations west and east of 86°W, respectively.

sets are independent (Figure 5), including 239, 72, 123, and 157 earthquakes, respectively. We picked FedNor and APT89 data separately and used preexisting picks for the Abitibi and TW∼ST arrays [*Rondenay et al.*, 2000a, 2000b; *Sol et al.*, 2002]. The resulting set of traveltime picks includes 4043 FedNor/CNSN picks, 474 APT89 picks, 2724 Abitibi picks, and 1412 TW∼ST picks for a total of 8653 traveltime measurements. Given the distribution of global seismicity within the correct distance range, event coverage for this study is excellent (Figure 5), and we do not believe that the recording period is a major limiting factor on our resolution.

[22] Relative traveltimes between stations were measured using multichannel cross-correlation [*VanDecar and Crosson*, 1991] in the 0.5- to 3.0-Hz band. Some large events were excessively oscillatory at high frequencies and were picked in the 0.2- to 2.0-Hz band instead; this required omitting the short-period stations from consideration. Instrument responses were not removed as only relative picks were required and the instrument responses were generally similar in the narrow passbands used; however, the response polarity of the short-period stations was found to be reversed relative to the broadband stations. Traveltime residuals for each station were approximated by subtracting the expected IASP91 arrival time and then subtracting event and station averages (simulating the event and station corrections calculated during tomographic inversion). Stereographic plots of these residuals (Figure 6) are useful for determining data coverage and coherency at each station, as well as detecting outliers. The plots also contain structural information, in that clusters of positive and negative residuals reflect relatively low-velocity and high-velocity structures, respec-

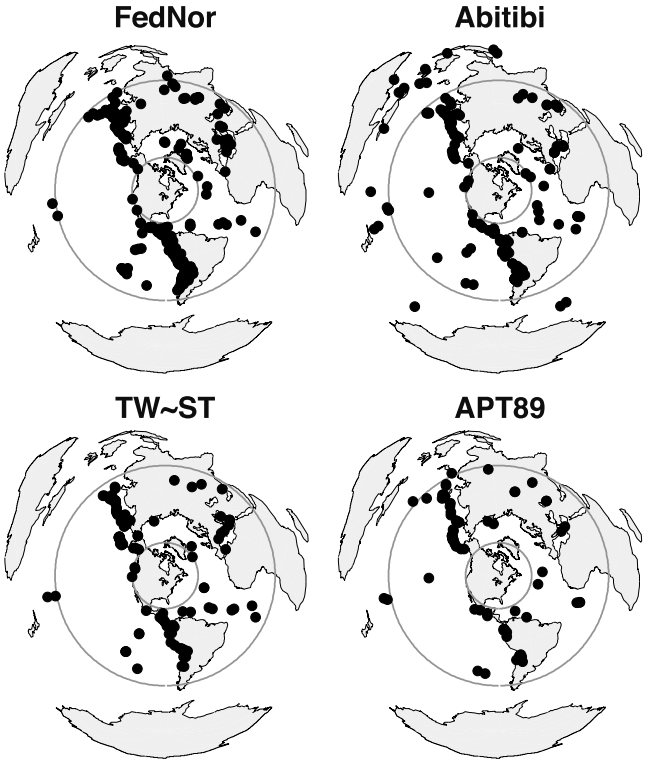

Figure 5. Distribution of events used in traveltime tomography for each of the station arrays. Gray circles indicate the approximate limits of the teleseismic range for *P* waves.

tively. Similar plots have been used as evidence for anisotropy [e.g., *Babuška and Plomerová*, 2006]; our reasons for interpreting the residual pattern as resulting from velocity structure are discussed in section 7.1.

6.3. Spatial Resolution

[23] Given the impracticality of directly calculating resolution matrices for large inverse problems, synthetic resolution tests are the generally accepted (albeit somewhat ad hoc) approach to determining the resolving power of a traveltime data set. We performed a series of resolution tests, aimed at quantifying the spatial resolution as well as determining the degree of smearing experienced by features similar to those recovered.

[24] We performed two checkerboard resolution tests, modeling traveltimes for a three-dimensional pattern of positive- and negative-velocity spikes 100 and 200 km apart (models A and B, respectively; Figure 7, upper left and lower left panels). Gaussian errors were added to the synthetic data to match the noise level interpreted to be present in the real data. As spikes and rapid polarity changes are heavily penalized by the model regularization, a checkerboard test represents a pessimistic estimate of the available resolution.

[25] The recovered model obtained by inverting the synthetic data (Figure 7, remaining panels) reproduces the alternating pattern of the input model. Resolution in body wave tomography requires crossing rays; given the limited station coverage in the middle of the model, resolution at 100-km depth (not shown) is restricted to eastern and western patches representing areas of dense station coverage. At greater depths, the raypaths diverge, evening out lateral resolution, though coverage at 150-km depth is still patchy; recovery of anomalies at 250- to 350-km depth is excellent and continues to 500 km (not shown). Given that anomalies 100 km apart are resolved (with some smearing), we interpret the lateral resolution of the core of our model to be 100–150 km from 200 km down to the base of the lithosphere; the excellent recovery of model B indicates that resolution is at least 200 km. Though the wide aperture of our station array provides coverage to greater depth, we will restrict our interpretation to the upper mantle (above the 410-km discontinuity). The amplitudes of small anomalies are significantly reduced in the recovered model (note the different velocity scale for model A output in Figure 7), while larger anomalies (model B) are recovered more accurately. The reduction in anomaly magnitude relative to the input model is a consequence of applying smoothing regularization to spike anomalies and indicates that the amplitudes of small features will be underestimated when inverting real data.

[26] Three structural resolution tests were performed (Figure 8), containing two low-velocity structures, a northwest trending channel in the southeastern quadrant of the study area and a spherical low-velocity anomaly 100 km in diameter centered underneath Lake Nipigon. In model C (which most closely matches the recovered model), the channel is 100 km wide and extends from the top of the model to 300-km depth, while the sphere is centered at 150-km depth; model D has shallower anomalies (the channel reaches 200-km depth, and the sphere is centered at 100 km), while model E has a narrower channel (50 km wide). Plan sections through the output models (Figure 8, top right and bottom right) show that the positions and lateral extents of the input structures are recovered very accurately; the shapes of the anomalies are not significantly altered, the channel's width is not significantly altered by smearing, and it is possible to distinguish 50- and 100-km-wide channels. Cross-sections (Figure 8, center right) indicate that some downward smearing has taken place, in that the bases of both anomalies are slightly lowered. The anomalies also tend to broaden at the very top of the model (where near-vertical raypaths limit the resolution); note that the top of the sphere in model C is not resolved. In all of the models, the magnitude of the channel anomaly is better recovered than that of the sphere, though both are underestimated.

[27] From these tests, we conclude that the resolution obtained by tomography follows a pattern typical for teleseismic traveltime experiments: the lateral resolution is very good, but vertical smearing occurs downward along raypaths. A series of "squeezing" tests, in which structure recovered from real data is restricted to lie above some limiting depth, did not cause significant shallowing of upper mantle anomalies, indicating that smearing is having a limited effect on the observed anomalies. In addition, a limiting depth of 270 km doubled the root mean square (RMS) traveltime misfit of the final model, indicating that the data require significant structure beneath the lithosphere. In general, we expect the widths of anomalies to be recovered fairly accurately and their depth extents to be

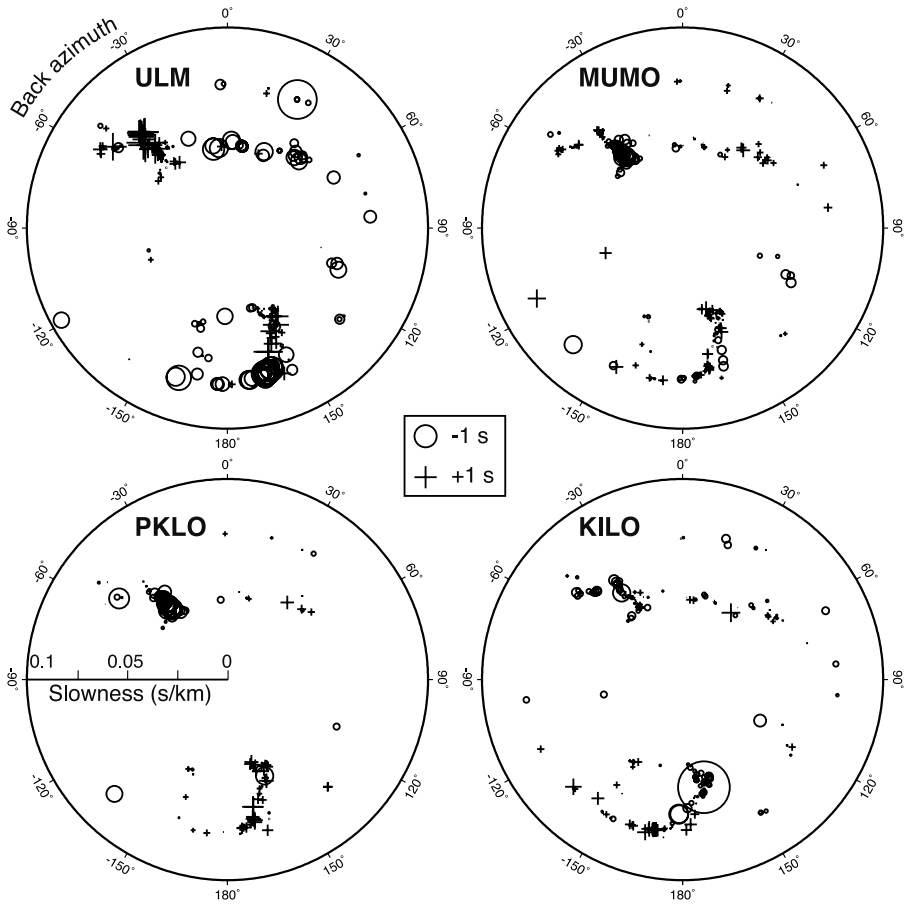

Figure 6. Traveltime residuals relative to IASP91 for four representative stations, with station and event averages subtracted. The residuals are plotted stereographically by the incoming ray angle; crosses represent positive residuals (late arrivals), while circles represent negative residuals (early arrivals). Note the positive residuals south of PKLO, indicating low-velocity structure, and the negative residuals to the northeast. Results for KILO include a prominent outlier (large circle to the south).

exaggerated by 50–100 km. We are also incapable of detecting the tops of anomalies that extend to depths shallower than 100 km.

6.4. Model

[28] Inversion results for the full data set are shown in Figures 9 and 10. A variance reduction of 99.7% was achieved using 20 robust iterations. Given past experience [*Frederiksen et al.*, 1998], velocity anomalies of less than 2% do not produce significant nonlinear (ray bending) effects, so ray tracing and nonlinear iteration were not performed. Recovered station time corrections (Figure 9) are small (RMS: 0.16 s, ranging from −0.49 to 0.55 s), while event time and location corrections are more substantial (RMS: 0.82 s, 39-km mean mislocation). The event time corrections compensate for structure in the source-side mantle, which may be a large contributor to the overall traveltime, while the station corrections correct for crustal structure and variations in instrument/site response and could potentially trade off with mantle structure within the model. A possible example of such trade-off is the large (−0.49 s) negative correction visible in the northeastern corner of Figure 9 (upper left panel), which may represent the mapping of fast arrivals (because of high-velocity mantle) into a large negative station correction. To limit this effect, the station corrections are regularized by damping and constrained to be zero-mean, while the event time corrections are undamped. Event mislocations are poorly constrained and are therefore also damped.

[29] Velocity perturbations in the model itself are not large, ranging from −1.9% to +1.8% relative to IASP91 in the upper 300 km of the model, the RMS perturbation being 0.48%. The major large-scale feature of the model is a division between high velocities in the west of the model and low velocities to the east, visible in all depth slices (Figures 9 and 10). The nature of the boundary varies somewhat between depth sections, but the dividing line between fast and slow mantle strikes approximately NNW-SSE between 85°W and 90°W. Below 350 km, the continuity of the boundary is largely lost (Figure 10), and the east-west division does not carry into the transition zone.

[30] At a smaller scale, the high- and low-velocity sections of the model are far from uniform. The high-velocity mantle beneath the western Superior has a lumpy appearance, with substantial local variation in velocity. The most significant of such variation is a small low-velocity anomaly centered at ≈50°N, 89°W, persisting to 300-km depth, which appears to be distinct from the larger low-velocity

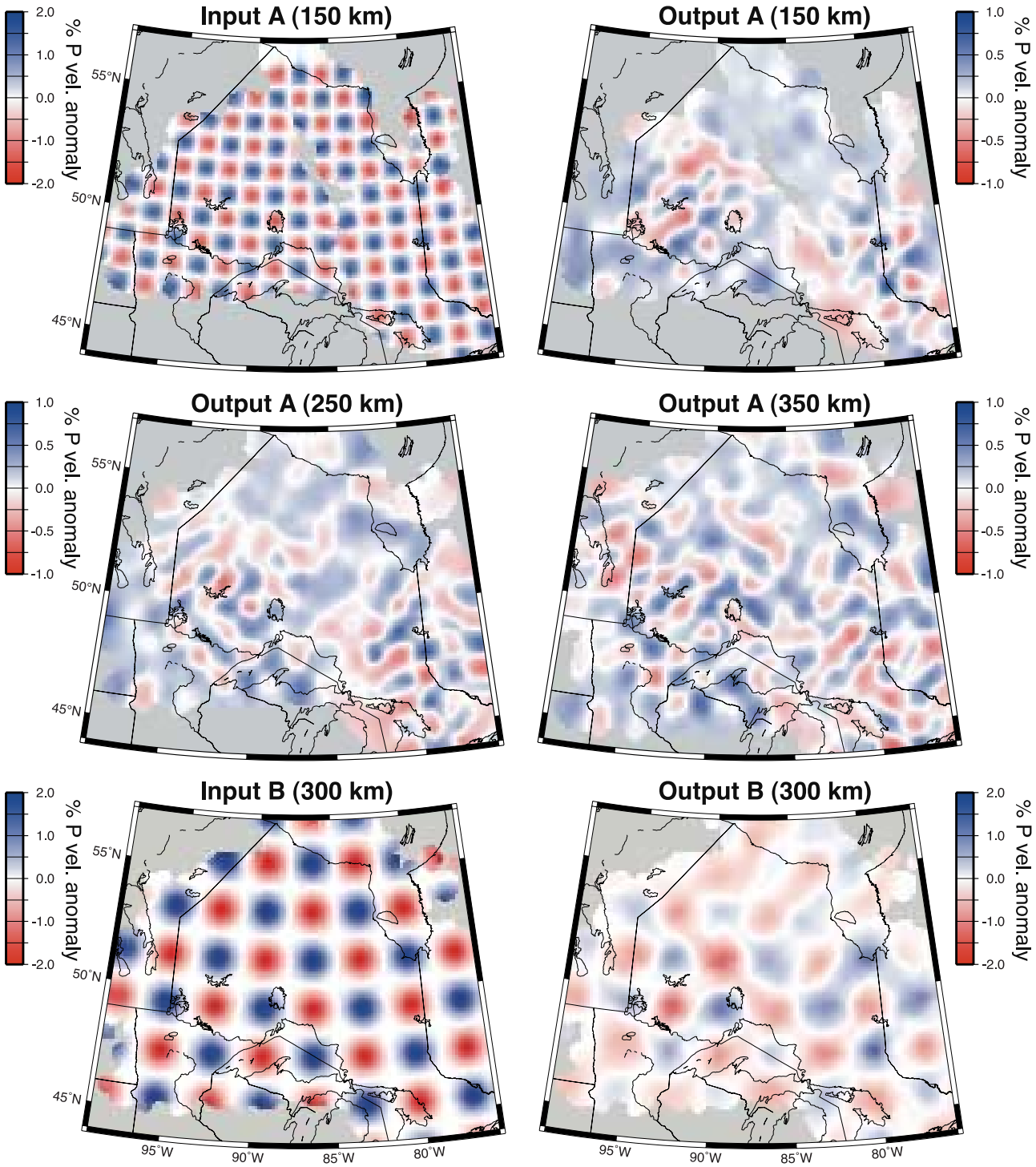

Figure 7. Resolution tests A and B for the tomographic data set. These tests used three-dimensional checkerboard patterns of alternating positive and negative spike anomalies; the anomalies were spaced 100 km apart in model A and 200 km apart in model B. The input models (top left and bottom left) were forward-modeled to generate simulated traveltime data, which were then inverted to obtain recovered models (other panels). Grayed-out regions have no significant ray coverage (ray density of less than 1).

region to the east. Immediately to its west is region of concentrated high velocities, the velocity change being ≈2.5% over a distance of 100–150 km. To the south, high velocities beneath Lake Superior are outside the region of station coverage and therefore may be an artifact; we will not interpret this feature.

[31] The major low-velocity region in the east of the model has a distinctly linear appearance with a clear

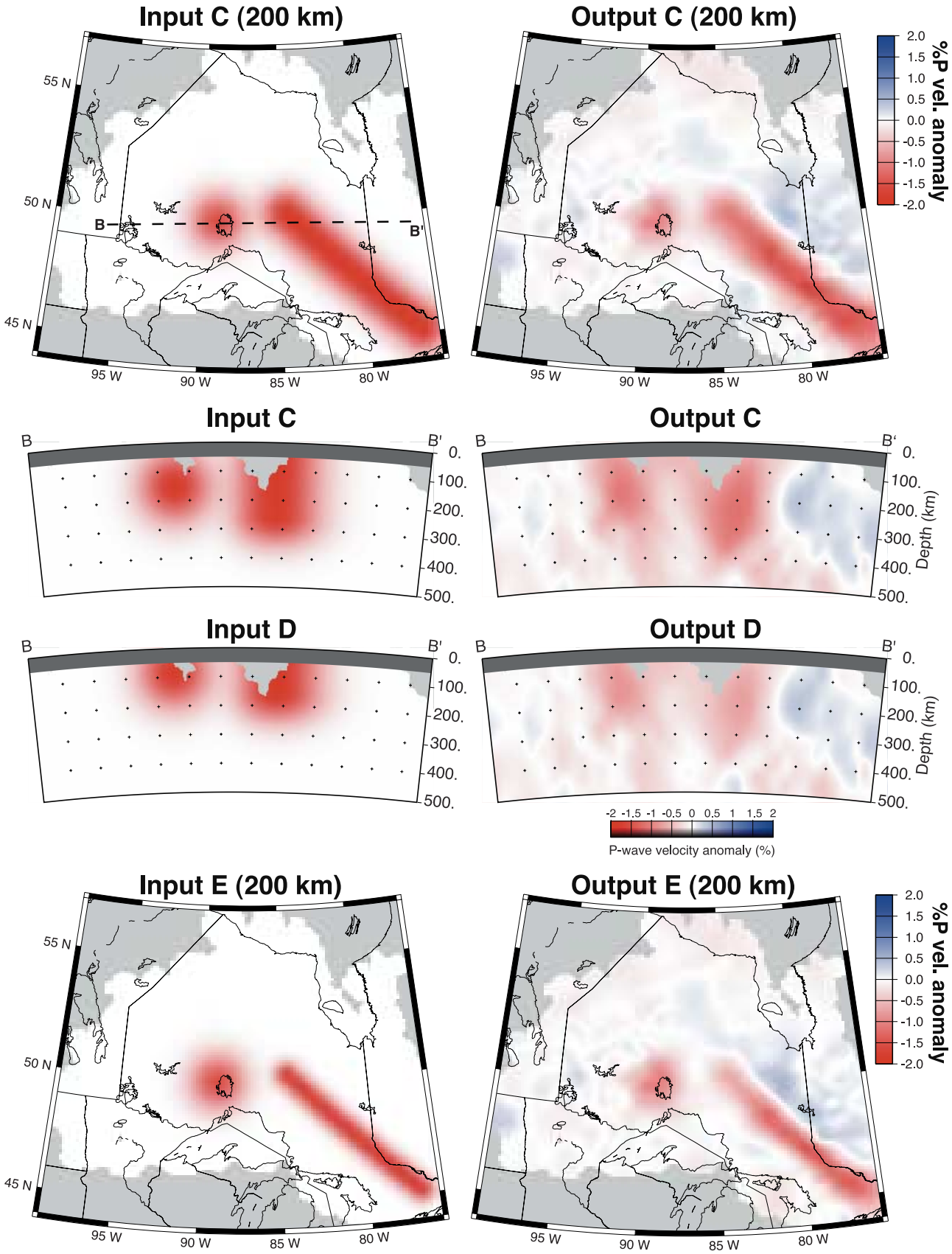
Input C (200 km)
Output C (200 km)
55 N
50 N
45 N
95 W
90 W
85 W
80 W
B
B'
2.0
1.5
1.0
0.5
0.0
-0.5
-1.0
-1.5
-2.0
%P vel. anomaly
Input C
Output C
Input D
Output D
0.
100.
200.
300.
400.
500.
Depth (km)
-2 -1.5 -1 -0.5 0 0.5 1 1.5 2
P-wave velocity anomaly (%)
Input E (200 km)
Output E (200 km)

Figure 8

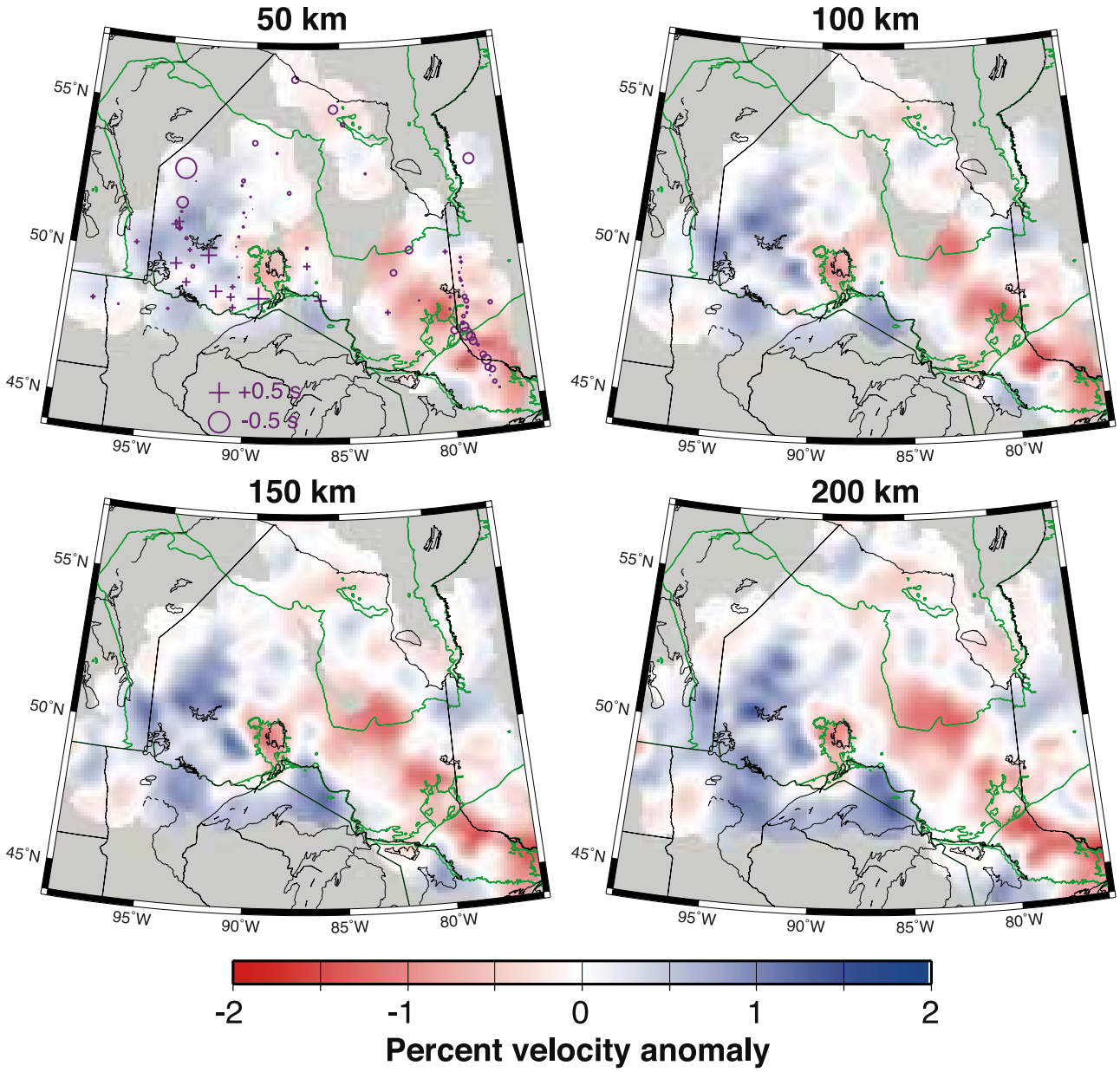

Figure 9. Plan sections through final three-dimensional model for depths from 50 to 200 km. Grayed-out regions have no significant ray coverage; green lines are tectonic province boundaries (from Figure 1a). Station time corrections are shown in purple on the 50-km section.

NW-SE trend. The linear anomaly forms a vertical sheet with no clearly preferred dip direction, becoming wider and more diffuse to the northeast. There is no sharp truncation, but the linear feature loses amplitude and disperses north of ≈50°N. East of this feature, the mantle velocity shows small variations but remains generally close to the IASP91 average above 300 km. The pattern of anomalies below 400 km in the eastern part of the model is different, but is beyond the scope of this lithospheric study and is of uncertain resolution.

7. Discussion

7.1. East-West Lithospheric Variations

[32] Visual inspection of Figure 11 shows that large SKS split times are well correlated with high velocities across the

Figure 8. Resolution tests C, D and E for the tomographic data set. These tests include structures similar to those recovered from the real data, a low-velocity channel in the southeast quadrant and a spherical low-velocity anomaly underlying Lake Nipigon. Model C includes a channel 100 km across, extending to 300-km depth, and a sphere 100 km in diameter centered at 150-km depth; model D terminates the low-velocity channel at 200-km depth and centers the sphere at 100 km. Model E is identical to C, except that the channel is 50 km across. Compare with Figures 9, 10, and 13.

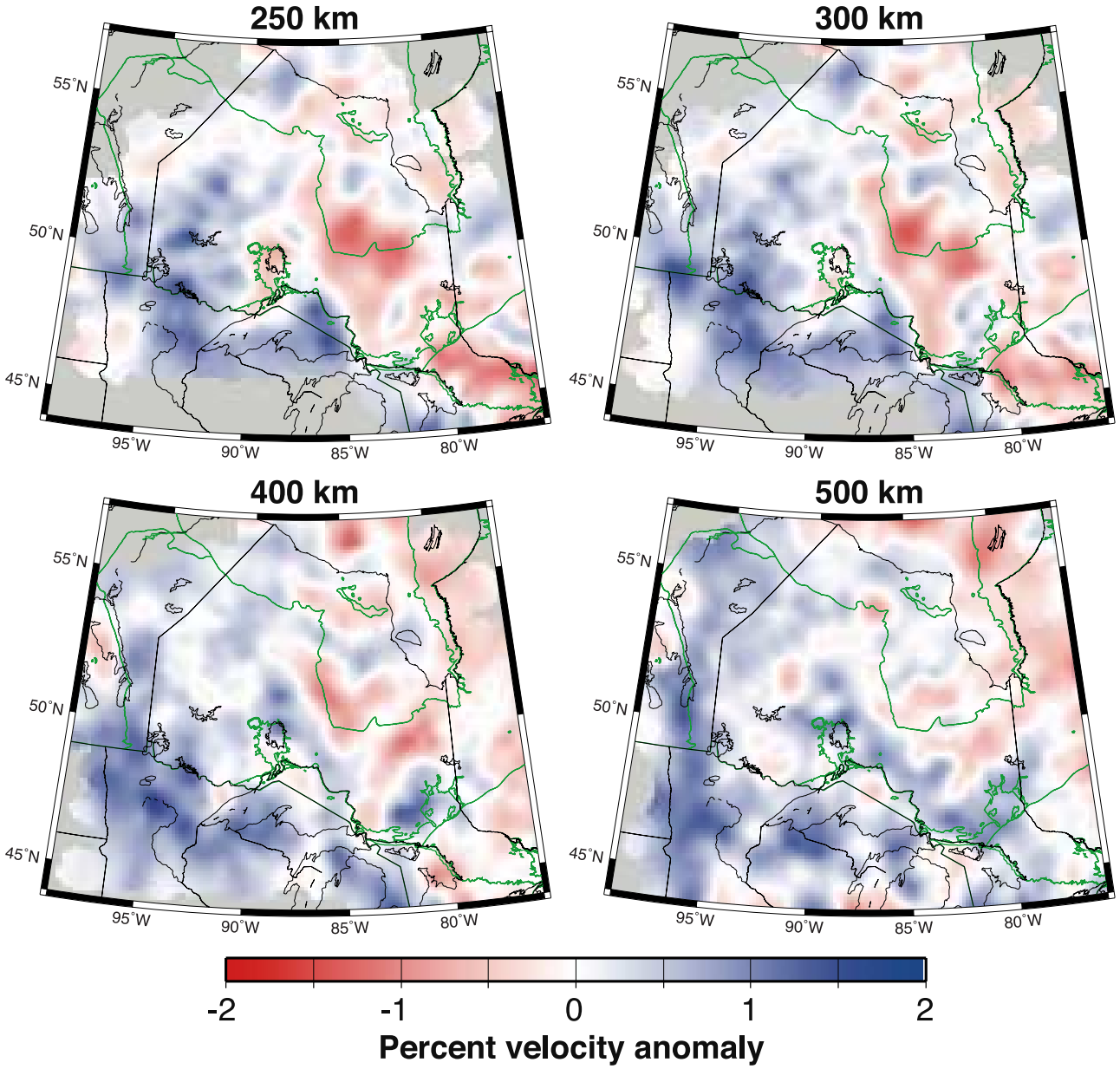

Figure 10. Plan sections through final three-dimensional model for depths from 250 to 500 km.

study area. The NNW-SSE boundary observed in the velocity model also serves to divide weaker SKS splits in the east from stronger splits in the west. We interpret this to represent a major change in the upper mantle between the western and eastern portions of the study area, the mantle beneath the western Superior being both high-velocity and strongly anisotropic, with a consistent ENE fast direction and split times greater than 1 s (reaching a maximum of 1.78 s at station EPLO). The interpreted boundary (dashed line in Figure 11) crosscuts subprovince boundaries (Figure 1) and is located west of the Kapuskasing Structural Zone, intersecting it at an angle of ≈45° near the eastern edge of Lake Superior.

[33] Given the strong anisotropy detected over most of the study area, and the close association between a major change in velocity and a major change in anisotropy, the possibility that the velocity change is an artifact of anisotropy must be addressed. A large-scale, consistent anisotropic fabric beneath a station will produce a characteristic bipolar pattern of residuals in back azimuth and slowness [e.g., *Babuška and Plomerová*, 2006]. *Bokelmann* [2002] showed that absolute *P* traveltime residuals from stations ULM and RSON (an older long-period station located near the current station RLKO) have a pattern consistent with upper mantle anisotropy, the fast axis trending SSW with a plunge of ≈18°. Our patterns of residuals, though coherent, do not exhibit this simple pattern (Figure 6). A likely explanation for this discrepancy is that we use relative rather than absolute traveltimes, which are sensitive to lateral changes in velocity rather than absolute velocity values; if the anisotropic pattern is identical between stations, it will not cause a relative traveltime difference. Bokelmann found a fairly uniform anisotropic pattern throughout the Canadian Shield, suggesting that distortions produced by such large-scale variations in *P* anisotropy are not large. Our SKS splitting results show a significant lateral anisotropy change,

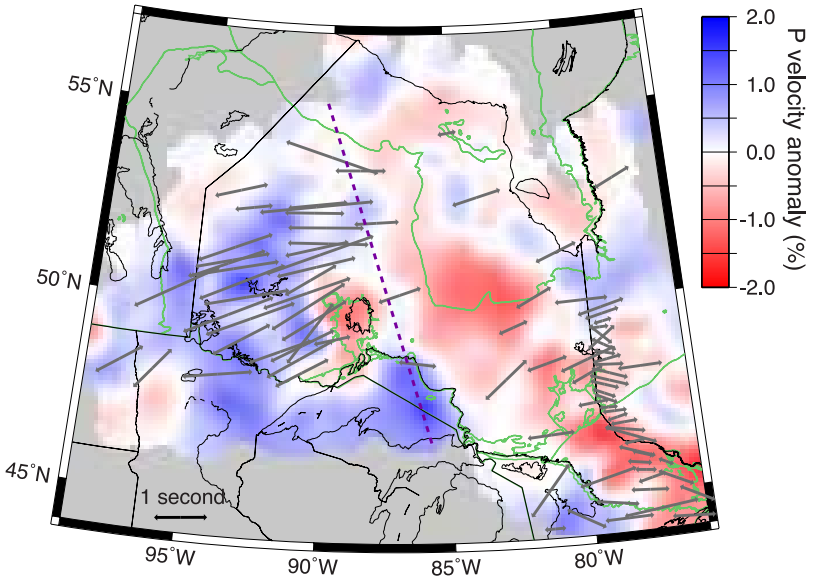

Figure 11. SKS splitting measurements from Figure 3, overlain on a 200-km slice through the final tomographic model. The dashed line represents the approximate location of an interpreted boundary between eastern and western mantle domains, based on split times and upper mantle velocity.

superimposed on an overall E-W to NE-SW pattern; it is unclear how much of an effect this would have on near-vertical *P* times, given that our splitting results have not constrained the plunge of the anisotropic symmetry axis. Given our broad distribution of back azimuths for *P* arrivals (Figure 5), the contribution of raypaths from a wide range of directions should help to cancel out any remaining anisotropic effect. Our results therefore provide strong evidence that the observed lithospheric boundary represents a major change in both isotropic velocity and anisotropic fabric.

[34] The depth of the anisotropy cannot be determined by SKS splitting alone. As can be seen in Figure 3, the fast directions detected in the Superior are largely subparallel to both the direction of absolute plate motion and to the orientation of tectonic belts. The intensive deformation involved in lithospheric accretion would be expected to generate lithospheric fabric in association with tectonic fabric, oriented in the direction of maximum extension or shear; *Silver and Kaneshima* [1993] and *Kay et al.* [1999] have argued that lithospheric fabric in the western Superior is aligned with Archean tectonic fabric, and thereby that the Superior lithosphere accreted in conjunction with the crust. Given that absolute plate motion determines the likely direction of asthenospheric shear, and assuming that the lithosphere's fabric is aligned with tectonic boundaries, lithospheric and asthenospheric fabrics are likely to be aligned over much of the Superior Province, and our observed SKS splits are consistent with both. *Silver and Kaneshima* [1993] compare split times to *S* traveltime residuals across the southwest boundary of the Superior and argue that the correlation between the two implies that much of the detected anisotropy is lithospheric in origin. Detailed Rayleigh-wave modeling along paths in the western Superior [*Darbyshire et al.*, 2006] found a systematic variation in *S* velocity with path orientation across the western Superior, indicating strong lithospheric anisotropy with a probably WSW-ENE fast direction, consistent with the observed splits. *Kay et al.* [1999] also argue for a lithospheric contribution in the western Superior, given regional variation in direction and the lack of observed splitting at stations on the Hudson's Bay coast. Across the Superior-Grenville boundary [*Fouch et al.*, 2000; *Eaton et al.*, 2004; *Frederiksen et al.*, 2006], there is evidence for enhanced asthenospheric anisotropy resulting from flow around a lithospheric "divot", as well as short-wavelength splitting variations attributable (by a Fresnel-zone argument; see e.g., *Frederiksen et al.* [2006]) to lithospheric structure. We consider it unlikely that there is no asthenospheric contribution to the observed splitting and therefore interpret the observed splits to result from aligned asthenospheric and lithospheric fabric. The large splits observed in the western Superior may indicate particularly close alignment, thick lithosphere, or enhanced lithospheric anisotropy related to tight spacing of tectonic subprovinces (Figure 3).

[35] Taking into account the considerations discussed above, we assume that the observed anisotropy and *P* velocity boundary is lithospheric in nature, representing a change of ≈0.7-s split time and ≈2% *P* velocity over ≈200–300 km. Given the tendency for vertical smearing of large anomalies in teleseismic traveltime tomography, we do not have good direct constraints on the lithospheric thickness beneath the Superior. The boundary appears to persist down to 400 km, which is an implausibly large value for lithospheric thickness; previous surface-wave analyses have returned more realistic values of 200–250 km [e.g., *Van der Lee and Frederiksen*, 2005], and we believe our model to be exaggerating depths by 50% or more. *Darbyshire et al.* [2006] found a high-velocity lithospheric lid 140–240 km thick beneath paths crossing the Superior Province, the thickest lithosphere underlying the northeast corner of Ontario, and did not observe a consistent E-W change in lithospheric thickness. The path-averaged models recovered by *Darbyshire et al.* [2006] are ill-suited to

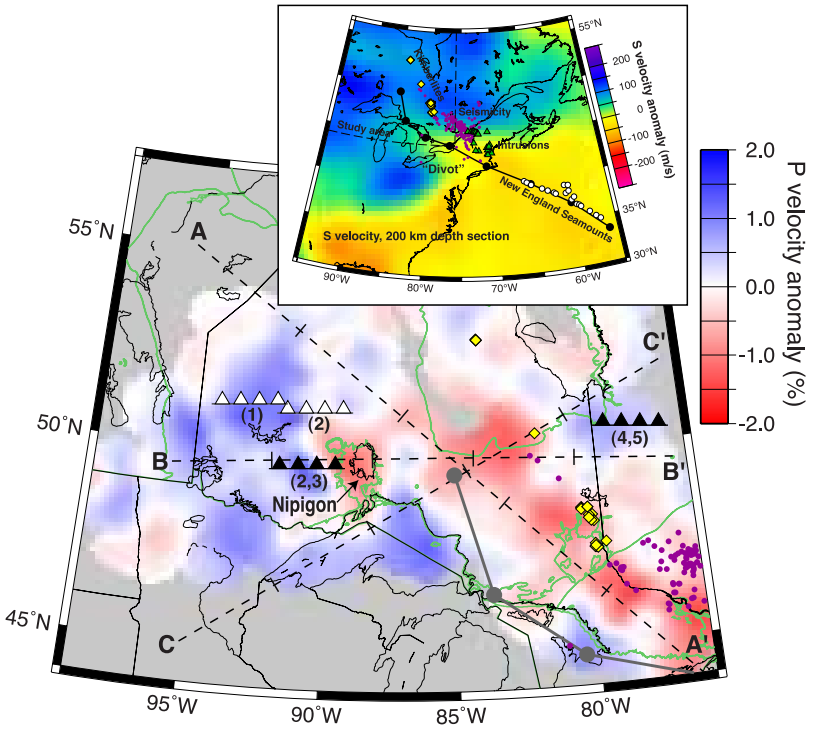

Figure 12. Main map: approximate locations of crustal-scale sutures detected by LITHOPROBE controlled-source experiments, superimposed on a 150-km slice through the final tomographic model. Sutures shown in solid black exhibited mantle reflectivity. References for the sutures are 1, *Calvert et al.* [2004]; 2, *White et al.* [2003]; 3, *Musacchio et al.* [2004]; 4, *Calvert et al.* [1995]; 5, *Calvert and Ludden* [1999]. Note the location of the Nipigon Embayment (green outline north of Lake Superior). Crustal features associated with the Great Meteor hot spot track [*Eaton and Frederiksen*, 2007] are plotted in the eastern half of the map: midcrustal seismicity (purple dots) and kimberlite occurrences (yellow diamonds). The gray line is the track of the hot spot as reconstructed by *Eaton and Frederiksen* [2007] by projecting the trend of the New England seamounts via a plate-motion reconstruction. Fine dashed lines indicate the locations of the cross-sections in Figure 13. Inset: eastward prolongation of the hot spot track, plotted on a surface-wave velocity model [*Eaton and Frederiksen*, 2007; *Van der Lee and Frederiksen*, 2005]. Note how the reconstructed track matches the low-velocity ''divot'', while the associated crustal features diverge.

localizing sharp lateral boundaries; western paths, however, did exhibit generally high lithospheric velocities. Given the surface-wave results and the absence of a distinct higher velocity layer overlying low velocities in the tomographic model, we cannot be certain that the observed boundary represents an increase in lithospheric thickness to the west; however, we are confident that the boundary represents a major change in lithospheric velocity.

7.2. Subduction Remnants and the Nipigon Embayment

[36] The preservation of remnant slabs during cratonic accretion has been proposed as a major contributor to the development of continental lithosphere. Provided that the lithosphere has not deformed significantly since its accretion, we would expect to detect remnant slabs in the vicinity of suture zones within the craton. The accretion of the Superior Province produced multiple suture zones along subprovince boundaries [*Card and Poulsen*, 1998], several of which were imaged by LITHOPROBE studies. Figure 12 shows the approximate locations of crustal-scale suture zones imaged by seismic reflection along the western Superior and Abitibi-Grenville transects [*Calvert et al.*, 1995; *Calvert and Ludden*, 1999; *White et al.*, 2003], some of which are associated with mantle reflectivity attributed to a remnant slab. Though the coverage of LITHOPROBE lines was by no means exhaustive and the mantle penetration of reflection data is limited, there is an interesting correspondence between suture locations determined by reflection and regions of high upper mantle velocity in our tomographic model. Assuming that this correspondence is not coincidental, the lithosphere beneath the sutures would need to be slightly but significantly faster than the surrounding continental lithosphere. Given the age of the sutures, such a contrast would have to be chemical in nature, perhaps indicating that the mantle near the sutures is further depleted relative to an already-depleted surrounding lithosphere. Such a relationship would lend support to the possibility that Archean subduction contributed to the development of a high-velocity lithosphere beneath the Superior Province and that the closer spacing of sutures in the western Superior may account in part for its higher velocities.

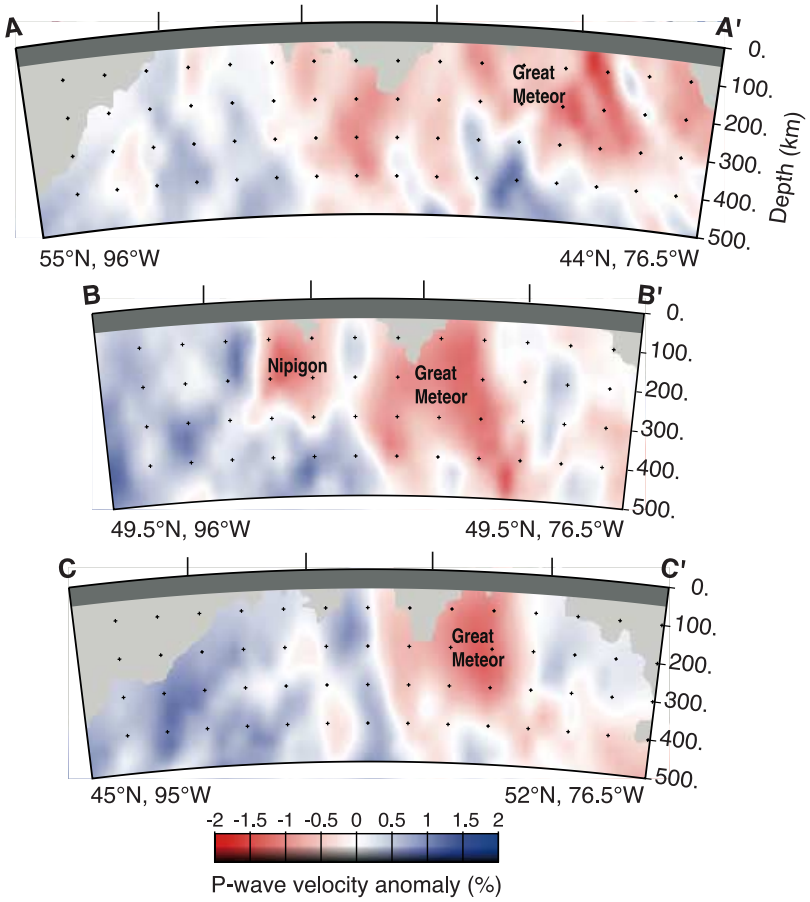

Figure 13. Three cross-sections through the final tomography model. The locations of the cross-sections are shown in Figure 12. The locations of the interpreted Nipigon Embayment and Great Meteor hot spot track anomalies are indicated.

[37] Better constraints on mantle structure were obtained in the western Superior using seismic refraction [*Musacchio et al.*, 2004]. This study located a high-velocity, anisotropic, north-dipping feature at 40- to 60-km depth in the upper mantle north of the Wawa-Quetico suture, interpreted to represent preserved oceanic lithosphere. Vertical propagation through this layer would produce a *P* residual of ≈ -0.23 s relative to IASP91, which is insufficient on its own to account for our observed anomaly (300 km of a 2% anomaly would generate a residual of ≈ -0.7 s). However, it is likely to be a contributor to the overall high velocity of the western Superior.

[38] A previous teleseismic tomography study by *Sol et al.* [2002], using only the TW$\sim$ST data, located a high-velocity mantle feature in the same general area as the slab feature located by *Musacchio et al.* [2004], albeit at considerably greater depth and with a NE dip. Sol et al. interpreted the high-velocity feature to represent a preserved slab and an adjacent low-velocity feature as a hydrated or altered mantle wedge above the slab. Our model (Figures 12 and 13) also includes these features, but with our broader coverage it is possible to see more of their three-dimensional geometry. The high-velocity anomaly previously interpreted as a slab now appears to connect to a larger high-velocity zone to the west, though the velocities are locally high in the region discussed by Sol et al. (centered at $\approx$49°N by 91°W). Although preservation of slab material in the lithospheric mantle is consistent with local high velocities, the said slab would only be a part of a larger high-velocity structure underlying much of the western Superior Province.

[39] Given our broader coverage, it is clear that the low-velocity feature detected by *Sol et al.* [2002] east of the presumed slab continues further east than previously thought. In fact, its outline corresponds nearly exactly (given the resolution of our model) to the boundaries of the Nipigon Embayment (Figure 12). Barring an unlikely coincidence, this correspondence implies that the mantle feature we observe is related to the (Proterozoic) embayment, and therefore not to the (presumably Archean) slab. The Nipigon Embayment [*Sutcliffe*, 1991] has been interpreted as a failed arm of the Midcontinent Rift, and the low velocities beneath it may reflect localized lithospheric thinning related to rifting. Allowing for the degree of downward smearing seen in Figure 8, the low-velocity anomaly beneath the Nipigon Embayment extends to at least 200-km depth (Figure 13, section B–B′), which is in line with previous lithospheric thickness estimates; it may therefore reflect a region in which the lithosphere was thinned by extension and replaced by asthenospheric mate-

rial. The embayment also appears as a region of anomalous magnetotelluric phase [*Ferguson et al.*, 2005] at frequencies corresponding to mantle depths. It is curious that the embayment is underlain by low-velocity material, while the main part of the rift (beneath Lake Superior) appears as a high-velocity region in our model; however, Lake Superior lies outside of our station coverage, resulting in a lack of crossing raypaths and poor resolution. As a result, the high velocities beneath Lake Superior may be an artifact of structure outside the model region, smeared upward along ray paths.

7.3. Great Meteor Hot Spot Track

[40] The lowest velocities in the eastern portion of the study area form a linear track ≈250 km wide (Figure 12), extending to a depth of 250–300 km allowing for smearing artifacts (Figure 13; section A–A′ lies along the track, while C–C′ is perpendicular). This track is the continuation of a feature seen in studies of the Abitibi-Grenville data [*Rondenay et al.*, 2000a, 2000b] and POLARIS data from southern Ontario [*Aktas and Eaton*, 2006]. Our results extend this feature to ≈87°W in the central Superior, where it appears to widen somewhat; the structural resolution tests in Figure 8 imply that the widening is not a smearing artifact. The track does not appear to extend into the western Superior; therefore, we believe that we have located the northwestern end of the linear feature.

[41] *Rondenay et al.* [2000a, 2000b] associated the low-velocity track with a southeast-younging trend of alkaline volcanism, including the Rapide des Quinze and Kirkland Lake kimberlites, the Monteregian and White Mountains intrusions, and the New England seamounts. They interpreted the volcanism trend and low-velocity anomaly as representing the crust and mantle expressions of the Great Meteor hot spot track, generated by plate motion over a fixed or slow-moving hot spot, the plate being weakened by previous rifting episodes. *Heaman and Kjarsgaard* [2000] documented a kimberlite age progression consistent with the hot spot track model. Assuming this is the correct interpretation, our observation that the track ends in the central Superior Province is fairly consistent with the location of the oldest, northwesternmost kimberlites [*Heaman and Kjarsgaard*, 2000]. The widening of the track to the northwest could reflect diffusion of the anomaly over time [*Eaton and Frederiksen*, 2007]. Given the absence of supporting evidence for plume initiation, and given that the plume track is not necessarily preserved everywhere, we cannot state with confidence that the Great Meteor hot spot first appeared in the central Superior.

[42] A similar low-velocity feature is also visible in continental-scale surface-wave models [e.g., *Van der Lee and Frederiksen*, 2005], appearing as a low-velocity "divot" in the lithosphere. The anomaly we have detected is broadly consistent with the location (though not the width) of the surface-wave anomaly and extends the feature ≈200 km north of its previous limit of detection. *Eaton and Frederiksen* [2007] noted that the "divot" is aligned with the New England seamounts and the reconstructed track of the hot spot, but lies southwest of the crustal track within the continent (Figure 12, inset). They interpret this to represent a misalignment between the mantle and crustal tracks, indicating lithospheric creep driven by asthenospheric forcing. The low-velocity channel we have detected is also somewhat misaligned with the kimberlite locations and crustal seismicity associated with the track, which generally lie at or beyond the eastern edge of the channel (Figure 12). The misalignment is, however, weaker than that observed in the surface-wave image. We do not observe a westward or southwestward dip in the track (Figure 13), as would be expected in the case of uniform shear. This inconsistency could be resolved by accommodating the shear deformation in thin horizontal shear planes, which could explain the presence of thin, highly anisotropic layers in the lithosphere detected by receiver functions [*Frederiksen et al.*, 2006]. Alternatively, another mechanism for the misalignment could be invoked, such as deflection of upwelling around resistant lithosphere in the western Superior, though the deflection appears to begin well east of the lithospheric boundary. The apparent age progression in the misalignment appears to show an age progression in the surface-wave image [*Eaton and Frederiksen*, 2007], which is difficult to explain without invoking lithospheric shear.

7.4. Lithospheric Properties and Origin of Variations

[43] The different anomalies detected in this experiment require a range of possibly contradictory lithospheric properties. The high velocities in the western Superior, particularly where associated with Archean suture zones, imply long-term lithospheric stability and a close association with crustal structure. The boundary between the eastern and western regions of the study area is unlikely to represent a major change in mantle temperature, given the generally consistent heat flow values across the Canadian Shield [*Rolandone et al.*, 2003], making a compositional difference more likely. The Nipigon Embayment anomaly is too old (ca. 1 Ga) to be thermal in nature, displaying heat flow values close to the Canadian Shield average [*Perry et al.*, 2004]; we interpret it to represent relatively enriched asthenospheric material emplaced by rifting and then incorporated into the modern lithosphere. The close correspondence between the edges of the low-velocity anomaly and the crustal boundary of the Nipigon Embayment indicates that the lithosphere in the western Superior has been stable with respect to the crust for at least 1 Ga.

[44] The temperature and long-term stability of the lithosphere beneath the eastern portion of the study area is less clear. On the basis of thermal modeling, the Great Meteor plume track could still retain a thermal signature [*Eaton and Frederiksen*, 2007], though the lack of a heat flow change across the east-west boundary suggests that the eastern lithosphere is not hotter as a whole. *Rondenay et al.* [2000a] argue for a combination of decompressional melting, anisotropy, and iron enrichment to explain the low observed velocities in the channel. Using the Nipigon anomaly (which we have argued to be compositional in origin) as a baseline, the significantly higher magnitude of the hot spot track suggests that some thermal contribution is likely.

[45] The contrast between the stability of the Nipigon anomaly and the misalignment of the plume track with respect to their respective crustal manifestations presents a

puzzle. Both low-velocity anomalies reach similar basal depths (though note that we have not imaged the top of either feature), and the Nipigon anomaly is substantially older. Assuming that the entire study area is subjected to a similar level of basal shear, the only possible mechanism for the younger feature to experience more deformation than the older feature is a difference in rheology. We therefore infer that the difference between the eastern and western lithosphere is one of mechanical strength as well as *P* velocity. We propose a model in which the presence of closely spaced slabs (associated with tightly grouped tectonic belts and sutures) reinforces the western Superior lithosphere, stabilizing it and rendering it resistant to shear down to 200 km (the thickness of the Nipigon anomaly). The Nipigon anomaly, being too small to weaken the lithosphere significantly, is therefore maintained in place by the stronger material around it. There could be significant shear taking place below 200 km, though we do not have any direct evidence for this; the direction of shear inferred by *Eaton and Frederiksen* [2007] is parallel to the observed SKS splitting direction and may incorporate the effect of an intensely sheared layer at the base of the lithosphere (similarly to the model of *Bokelmann and Silver* [2002]). Support for a strong western Superior lithosphere is given by the extremely high elastic plate thickness obtained from gravity analysis [*Wang and Mareschal*, 1999], which reaches a maximum of ≈100 km in an anomaly centered in western Ontario.

[46] The lower overall velocity, weaker splitting, and inferred mechanical weakness in the eastern part of the study area remain to be explained. Though the lowest velocities lie within the Great Meteor track, the whole of the east has lower velocity than the west. Given that the only well-resolved positive velocity anomaly in the east coincides with a previously detected mantle slab (Figure 12), it is possible that some of the difference predates the passage of the hot spot and is a consequence of the more widely spaced tectonic belts in the east; however, the closest spacing of lithospheric belts occurs in the vicinity of the mantle boundary. Alternatively, passage of the hot spot may have eroded or modified the eastern lithosphere over a larger area than previously recognized. More detailed thermal and mechanical modeling will be required to determine the plausibility of plume activity producing a change in velocity and rheology over such a large area; we do not have sufficient constraints to resolve the issue at this time.

8. Conclusions

[47] Through a combination of SKS splitting analysis and teleseismic *P* tomography applied to a collection of broadband data from multiple experiments, we have recognized a new, profound east-west change in properties of the Superior craton at ≈86–88°W. The upper mantle west of ≈86–88°W displays high velocities throughout the lithosphere, elevated split times (averaging 1.3 s), and ENE-WSW fast directions. By contrast, the eastern part of the study area shows lower seismic velocities and split times, with more scattered fast directions averaging to an east-west orientation. The boundary does not correspond to any obvious crustal feature.

[48] West of the interpreted boundary, a low-velocity mantle anomaly closely corresponds to the crustal extent of the ≈1.0 Ga Nipigon Embayment, a failed branch of the Midcontinent Rift. Given the age of the embayment and the absence of a heat flow anomaly, we interpret this mantle feature to be purely chemical in origin and to represent an in situ compositional change resulting from rifting in the embayment. The Nipigon feature thus provides a useful calibration of the sensitivity of *P* velocity to purely chemical changes, and its close association with a crustal feature indicates that the lithosphere in the western Superior has been stable since 1 Ga. Localized high velocities associated with crustal sutures within the western Superior may represent remnant slabs related to accretion of the Superior Province, in which case the period of stability may be extended to ≈2.5–2.7 Ga.

[49] We interpret a linear low-velocity feature in the eastern portion of the model to be associated with the Great Meteor hot spot track, in agreement with previous studies. Our model provides evidence that the track extends well into the Superior craton (up to ≈52°N), in accordance with kimberlite studies [*Heaman and Kjarsgaard*, 2000]. Unlike the Nipigon anomaly, the hot spot track is offset to the west of associated crustal features, supporting the proposal by *Eaton and Frederiksen* [2007] that lithospheric deformation has occurred in the last ≈170 Ma. This would require a major difference in history, stability, and rheology between the eastern and western Superior, suggesting that the observed boundary between east and west corresponds to a change in mechanical strength. We propose a model in which the western Superior has undergone little deformation in its upper 200 km, while the weaker eastern Superior has been sheared by basal traction. This model could be better constrained by obtaining better depth constraints on anisotropy, particularly if the deformation of the eastern Superior is accommodated by relatively thin shear layers.

[50] **Acknowledgments.** We are grateful to FedNor, the POLARIS consortium, and the Geological Survey of Canada for funding data collection, overseeing instrument installation, and archiving data for the FedNor array. We would particularly like to acknowledge the participation of Kadircan Aktas, Isa Asudeh, and all members of the instrument deployment crews. SKS splitting analysis at station ULM was performed by Ashley Krakowka; fruitful discussions with Ian Ferguson as well as reviews by Vadim Levin and an anonymous reviewer led to substantial improvements in this manuscript. This research was funded by NSERC grants.

References

Aktas, K., and D. W. Eaton (2006), Upper-mantle velocity structure of the lower Great Lakes region, *Tectonophysics*, *420*, 267–281.

Babuška, V., and J. Plomerová (2006), European mantle lithosphere assembled from rigid microplates with inherited seismic anisotropy, *Phys. Earth Planet. Inter.*, *58*, 264–280.

Benn, K. (2006), Tectonic delamination of the lower crust during Late Archean collision of the Abitibi-Opatica and Pontiac terranes, Superior Province, Canada, in *Archean Geodynamics and Environments, Geophysical Monograph*, vol. 164, edited by K. Benn, J.-C. Mareschal, and K. Condie, pp. 267–282, AGU, Washington D.C.

Boerner, D. E., R. D. Kurtz, and J. A. Craven (2000), A summary of electromagnetic studies on the Abitibi-Grenville transect, *Can. J. Earth Sci.*, *37*, 427–437.

Bokelmann, G. (2002), Convection-driven motion of the North American craton: Evidence from *P*-wave anisotropy, *Geophys. J. Int.*, *148*, 278–287.

Bokelmann, G., and P. G. Silver (2000), Mantle variation within the Canadian Shield: Travel times from the portable broadband Archean-Proterozoic Transect 1989, *J. Geophys. Res.*, *105*, 579–605.

Bokelmann, G., and P. G. Silver (2002), Shear stress at the base of shield lithosphere, *Geophys. Res. Lett.*, *29*(23), 2091, doi:10.1029/2002GL015925.

Calvert, A. J., and J. N. Ludden (1999), Archean continental assembly in the southeastern Superior Province of Canada, *Tectonics*, *18*, 412–429.

Calvert, A. J., E. W. Sawyer, W. J. Davis, and J. N. Ludden (1995), Archean subduction inferred from seismic images of a mantle suture in the Superior Province, *Nature*, *375*, 670–674.

Calvert, A. J., A. R. Cruden, and A. Hynes (2004), Seismic evidence for preservation of the Archean Uchi granite-greenstone belt by crustal-scale extension, *Tectonophysics*, *388*, 135–143.

Card, K. D., and K. H. Poulsen (1998), Geology and mineral deposits of the Superior Province of the Canadian Shield, in *Geology of the Precambrian Superior and Grenville Provinces and Precambrian Fossils in North America, Geology of North America*, vol. C-1, edited by S. B. Lucas and M. R. St-Onge, pp. 13–204, Geological Survey of Canada, Ottawa.

Clowes, R. M., F. A. Cook, A. G. Green, C. E. Keen, J. N. Ludden, J. A. Percival, G. M. Quinlan, and G. F. West (1992), LITHOPROBE—New perspectives on crustal evolution, *Can. J. Earth Sci.*, *29*, 1813–1864.

Darbyshire, F. A., D. W. Eaton, A. W. Frederiksen, and L. Ertolahti (2006), New insights into the lithosphere beneath the Superior Province from Rayleigh wave dispersion and receiver function analysis, *Geophys. J. Int.*, in press.

Davidson, A. (1998), An overview of Grenville Province geology, Canadian Shield, in *Geology of the Precambrian Superior and Grenville Provinces and Precambrian Fossils in North America, Geology of North America*, vol. C-1, edited by S. B. Lucas and M. R. St-Onge, pp. 205–270, Geological Survey of Canada, Ottawa.

Eaton, D. W., and A. W. Frederiksen (2007), Seismic evidence for convection-driven motion of the North American plate, *Nature*, *446*, 428–431.

Eaton, D. W., A. W. Frederiksen, and S.-K. Miong (2004), Shear wave splitting observations in the lower Great Lakes region: Evidence for regional anisotropic domains and keel-modified asthenospheric flow, *Geophys. Res. Lett.*, *31*, L07610, doi:10.1029/2004GL019438.

Eaton, D. W., et al. (2005), Investigating Canada's lithosphere and earthquake hazards with portable arrays, *Eos Trans. AGU*, *86*, 160–173, doi:10.1029/2005EO170001.

Ferguson, I. J., et al. (2005), Geoelectric response of Archean lithosphere in the western Superior Province, central Canada, *Phys. Earth Planet. Inter.*, *150*, 123–142.

Fouch, M. J., K. M. Fischer, E. M. Parmentier, M. E. Wysession, and T. J. Clarke (2000), Shear wave splitting, continental keels, and patterns of mantle flow, *J. Geophys. Res.*, *105*, 6255–6275.

Frederiksen, A. W., M. G. Bostock, J. C. VanDecar, and J. F. Cassidy (1998), Seismic structure of the upper mantle beneath the northern Canadian Cordillera from teleseismic travel-time inversion, *Tectonophysics*, *294*, 43–55.

Frederiksen, A. W., I. J. Ferguson, D. Eaton, S.-K. Miong, and E. Gowan (2006), Mantle fabric at multiple scales across an Archean-Proterozoic boundary, Eastern Ontario, Canada, *Phys. Earth Planet. Inter.*, *158*, 240–263.

Godey, S., R. Snieder, A. Villaseñor, and H. M. Benz (2003), Surface wave tomography of North America and the Caribbean using global and regional broad-band networks: Phase velocity maps and limitations of ray theory, *Geophys. J. Int.*, *152*, 620–632.

Green, J. C., T. J. Bonhorst, V. W. Chandler, M. G. Mudrey Jr., P. E. Myers, L. J. Pesonen, and J. T. Wilband (1987), Keweenawan dykes of the Lake Superior region: Evidence for evolution of the Middle Proterozoic Midcontinent Rift of North America, in *Mafic Dyke Swarms, Geological Association of Canada Special Paper 34*, edited by H. C. Halls and W. F. Fahrig, pp. 289–302, Geological Association of Canada, Toronto.

Heaman, L. M., and B. A. Kjarsgaard (2000), Timing of eastern North American kimberlite magmatism: Continental extension of the Great Meteor hotspot track?, *Earth Planet. Sci. Lett.*, *178*, 253–268.

Ji, S., S. Rondenay, M. Mareschal, and G. Sénéchal (1996), Obliquity between seismic and electrical anisotropies as a potential indicator of movement sense for ductile shear zones in the upper mantle, *Geology*, *24*, 1033–1036.

Jordan, T. H. (1978), Composition and development of the continental tectosphere, *Nature*, *274*, 544–548.

Jordan, T. H. (1988), Structure and formation of the continental tectosphere, *J. Petrol. Special Lithosphere Issue*, 11–37.

Kay, I., S. Sol, J.-M. Kendall, C. Thompson, D. White, I. Asudeh, B. Roberts, and D. Francis (1999), Shear wave splitting observations in the Archean craton of Western Superior, *Geophys. Res. Lett.*, *26*, 2669–2672.

Kennett, B. L. N., and E. R. Engdahl (1991), Traveltimes for global earthquake location and phase identification, *Geophys. J. Int.*, *105*, 429–465.

Larson, K. M., J. T. Freymueller, and S. Philipsen (1997), Global plate velocities from the Global Positioning System, *J. Geophys. Res.*, *102*, 9961–9981.

Levin, V., W. Menke, and J. Park (1999), Shear wave splitting in the Appalachians and the Urals: A case for multilayered anisotropy, *J. Geophys. Res.*, *104*, 17,975–17,993.

Lucas, S. B., M. R. St-Onge, and J. A. Percival (1998), Introduction, in *Geology of the Precambrian Superior and Grenville Provinces and Precambrian Fossils in North America, Geology of North America*, vol. C-1, edited by S. B. Lucas and M. R. St-Onge, pp. 1–12, Geological Survey of Canada, Ottawa.

Musacchio, G., D. J. White, I. Asudeh, and C. J. Thomson (2004), Lithospheric structure and composition of the Archean western Superior Province from seismic refraction/wide-angle reflection and gravity modelling, *J. Geophys. Res.*, *109*, B03304, doi:10.1029/2003JB002427.

Osmani, I. A. (1991), Proterozoic mafic dyke swarms in the Superior Province of Ontario, in *Geology of Ontario, Ontario Geological Survey Special Volume 4, Part 1*, edited by P. C. Thurston, H. R. Williams, R. H. Sutcliffe, and G. M. Stott, pp. 661–681, Ontario Geological Survey, Toronto.

Parker, R. L. (1994), *Geophysical Inverse Theory*, 366 pp., Princeton Univ. Press, Princeton, N.J.

Pearson, D. G. (1999), The age of continental roots, *Lithos*, *48*, 171–194.

Percival, J. A., and G. F. West (1994), The Kapuskasing uplift: A geological and geophysical synthesis, *Can. J. Earth Sci.*, *31*, 1256–1286.

Perry, H. K. C., C. Jaupart, J.-C. Mareschal, F. Rolandone, and G. Bienfait (2004), Heat flow in the Nipigon Arm of the Keweenawan rift, northwestern Ontario, Canada, *Geophys. Res. Lett.*, *31*, L15607, doi:10.1029/2004GL020159.

Rolandone, F., J.-C. Mareschal, C. Jaupart, C. Gosselin, G. Bienfait, and R. Lapointe (2003), Heat flow in the western Superior Province of the Canadian shield, *Geophys. Res. Lett.*, *30*(12), 1637, doi:10.1029/2003GL017386.

Rondenay, S., M. G. Bostock, T. M. Hearn, D. J. White, and R. M. Ellis (2000a), Lithospheric assembly and modification of the SE Canadian Shield: Abitibi-Grenville teleseismic experiment, *J. Geophys. Res.*, *105*, 13,735–13,754.

Rondenay, S., M. G. Bostock, T. M. Hearn, D. J. White, H. Wu, G. Sénéchal, S. Ji, and M. Mareschal (2000b), Teleseismic studies of the lithosphere below the Abitibi-Grenville Lithoprobe transect, *Can. J. Earth Sci.*, *37*, 415–426.

Silver, P. G., and W. W. Chan (1991), Shear wave splitting and subcontinental mantle deformation, *J. Geophys. Res.*, *96*, 16,429–16,454.

Silver, P. G., and S. Kaneshima (1993), Constraints on mantle anisotropy beneath Precambrian North America from a transportable teleseismic experiment, *J. Geophys. Res.*, *20*, 1127–1130.

Silver, P. G., R. P. Meyer, and D. E. James (1993), Intermediate-scale observations of the Earth's deep interior from the APT89 transportable teleseismic experiment, *Geophys. Res. Lett.*, *20*, 1123–1126.

Sobolev, S. V., H. Zeyen, G. Stoll, F. Werling, R. Altherr, and K. Fuchs (1996), Upper mantle temperatures from teleseismic tomography of French Massif Central including effects of composition, mineral reactions, anharmonicity, anelasticity and partial melt, *Earth Planet. Sci. Lett.*, *139*, 147–163.

Sol, S., C. J. Thomson, J.-M. Kendall, D. White, J. C. VanDecar, and I. Asudeh (2002), Seismic tomographic images of the cratonic upper mantle beneath the Western Superior Province of the Canadian Shield—A remnant Archean slab?, *Phys. Earth Planet. Inter.*, *134*, 53–69.

Sutcliffe, R. H. (1991), Proterozoic geology of the Lake Superior area, in *Geology of Ontario, Ontario Geological Survey Special Volume 4, Part 1*, edited by P. C. Thurston, H. R. Williams, R. H. Sutcliffe, and G. M. Stott, pp. 627–658, Ontario Geological Survey, Toronto.

Thurston, P. C. (1991), Proterozoic geology of Ontario: Introduction, in *Geology of Ontario, Ontario Geological Survey Special Volume 4, Part 1*, edited by P. C. Thurston, H. R. Williams, R. H. Sutcliffe, and G. M. Stott, pp. 543–546, Ontario Geological Survey, Toronto.

VanDecar, J. (1991), Upper-mantle structure of the Cascadia subduction zone from non-linear teleseismic travel-time inversion, Ph.D. thesis, 165 pp., Univ. of Wash., Seattle, Wash.

VanDecar, J. C., and R. S. Crosson (1991), Determination of teleseismic relative phase arrival times using multi-channel cross correlation and least squares, *Bull. Seismol. Soc. Am.*, *80*, 150–169.

VanDecar, J. C., D. E. James, and M. Assumpcão (1995), Seismic evidence for coherent flow of the crust and upper mantle below South America since the breakup of Gondwana, *Nature*, *378*, 25–31.

Van der Lee, S., and A. Frederiksen (2005), Surface wave tomography applied to the North American upper mantle, in *Seismic Earth: Array Analysis of Broadband Seismograms, Geophysical Monograph*,

vol. 157, edited by A. Levander and G. Nolet, pp. 67–80, AGU, Washington D.C.

Wang, Y., and J.-C. Mareschal (1999), Elastic thickness of the lithosphere in the central Canadian Shield, *Geophys. Res. Lett.*, *26*, 3033–3035.

White, D. J., G. Musacchio, H. H. Helmstaedt, R. M. Harrap, P. C. Thurston, A. Van der Velden, and K. Hall (2003), Images of a lower-crustal oceanic slab: Direct evidence for tectonic accretion in the Archean western Superior province, *Geology*, *31*, 997–1000.

Williams, H. R., G. M. Stott, P. C. Thurston, R. H. Sutcliffe, G. Bennett, R. M. Easton, and D. K. Armstrong (1991), Tectonic evolution of Ontario: Summary and synthesis, in *Geology of Ontario, Ontario Geological Survey Special Volume 4, Part 2*, edited by P. C. Thurston, H. R. Williams, R. H. Sutcliffe, and G. M. Stott, pp. 1255–1332, Ontario Geological Survey, Toronto.

Wolfe, C. J., and P. G. Silver (1998), Seismic anisotropy of oceanic upper mantle: Shear wave splitting methodologies and observations, *J. Geophys. Res.*, *103*, 749–771.

Wu, J., and R. F. Mereu (1992), Crustal structure of the Kapuskasing Uplift from LITHOPROBE near-vertical/wide-angle seismic reflection data, *J. Geophys. Res.*, *97*, 17,441–17,453.

F. A. Darbyshire, Département des sciences de la terre et de l'atmosphere, Université du Québec à Montréal, Case postale 8888, Succursale Centre-ville, Montréal, Québec H3C 3P8, Canada. (f.darbyshire@gmail.com)

D. W. Eaton, Department of Earth Sciences, University of Western Ontario, London, Ontario N6A 5B7, Canada. (deaton@uwo.ca)

A. W. Frederiksen, Department of Geological Sciences, University of Manitoba, 341 Wallace Building Winnipeg, Manitoba R3T 2N2, Canada. (frederik@cc.umanitoba.ca)

S.-K. Miong, Department of Geology and Geophysics, University of Calgary, Calgary, Alberta T2N 1N4, Canada. (skmiong@ucalgary.ca)

S. Rondenay, Department of Earth, Atmospheric and Planetary Sciences, Massachusetts Institute of Technology, 77 Massachusetts Ave. 54-512, Cambridge, MA 02139, USA. (rondenay@mit.edu)

S. Sol, Department of Earth and Environmental Sciences, Lehigh University, 31 Williams Drive, Bethlehem, PA 18015, USA. (stsd@lehigh.edu)